Original Article

MOLECULAR METABOLISM

Disrupted liver oxidative metabolism in glycine N-methyltransferase-deficient mice is mitigated by dietary methionine restriction

Ferrol I. Rome, Curtis C. Hughey*

ABSTRACT

Objective: One-carbon metabolism is routinely dysregulated in nonalcoholic fatty liver disease. This includes decreased glycine N-methyltransferase (GNMT), a critical regulator of s-adenosylmethionine (SAM). Deletion of GNMT in mice increases SAM and promotes liver steatosis. Lower liver oxidative metabolism, as indicated by a decline in gluconeogenesis, citric acid cycle flux, and oxidative phosphorylation contributes to liver steatosis in GNMT-null mice; however, the extent to which higher SAM mediates this phenotype remains unclear. Here, we determined the SAM-dependent impairment in liver oxidative metabolism by loss of GNMT.

Methods: GNMT knockout (KO) mice were fed a methionine-restricted diet to prevent increased SAM. $^{2}H/^{13}C$ metabolic flux analysis was performed in conscious, unrestrained mice to quantify liver nutrient fluxes. Metabolomics and high-resolution respirometry were used to quantify liver nutrient pool sizes and mitochondrial oxidative phosphorylation, respectively. Folic acid-supplemented and serine/glycine-deficient diets were used independently to further define the metabolic implications of perturbed one-carbon donor availability.

Results: Dietary methionine restriction prevented a 75-fold increase in SAM and a 53% rise in triacylglycerides in livers of KO mice. Dietary methionine restriction increased gluconeogenesis, independent of genotype, and restored cytochrome c oxidase respiratory function in KO mice. Citric acid cycle fluxes remained lower in KO mice irrespective of diet. Restricting dietary methionine abrogated markers of increased lipogenesis and folate cycle dysfunction in KO mice.

Conclusions: The impaired liver oxidative metabolism following loss of GNMT is both dependent and independent of greater SAM availability. Lower *in vivo* citric acid cycle flux is independent of increased SAM. In contrast, gluconeogenesis and oxidative phosphorylation are negatively regulated by excess SAM. Lipid accumulation in livers of mice lacking GNMT is also linked to higher SAM.

Keywords Citric acid cycle; Gluconeogenesis; Oxidative phosphorylation; Nonalcoholic fatty liver disease; One-carbon metabolism; Lipogenesis

1. INTRODUCTION

Nonalcoholic fatty liver disease (NAFLD), the most prevalent chronic liver disease worldwide, includes nonalcoholic fatty liver (NAFL) and nonalcoholic steatohepatitis (NASH) [1–3]. Both NAFL and NASH are defined by liver steatosis; however, NASH is also characterized by inflammation, fibrosis, and hepatocyte damage and death [4–6]. Moreover, NASH is considered the progressive form of NAFLD as it increases the risk for developing advanced liver diseases such as hepatocellular carcinoma (HCC) [4–6]. Extensive investigation has shown that dysregulated oxidative metabolism contributes to the pathophysiology of NAFLD and HCC [7]. Liver oxidative metabolism refers to a cluster of processes including gluconeogenesis, β-oxidation, ketogenesis, citric acid cycle flux, and oxidative phosphorylation. These pathways are often increased early in a NAFL, prior to a progressive decline with advancing NASH and HCC [7–13]. Ultimately, the capacity of oxidative metabolism is insufficient to meet the demands for nutrient catabolism. This contributes to an imbalance between lipid disposal and accretion and thereby supports NAFLD pathogenesis [14].

Mouse models of NAFLD-associated HCC routinely show decreased expression of one-carbon metabolism enzymes such as glycine N-methyltransferase (GNMT) [15–20]. Moreover, GNMT expression is lower or absent in human NAFLD and HCC [15,17,21–26]. GNMT, the most abundant liver methyltransferase, catalyzes the transfer of a methyl group from s-adenosylmethionine (SAM) to glycine, forming sarcosine and s-adenosylhomocysteine (SAH) [27]. This reaction is critical for SAM homeostasis, as GNMT-null mice exhibit liver SAM levels that are >35-fold higher than wild-type (WT) mice [28–31]. Previous studies support a causal role for the diminished GNMT in NAFLD and HCC pathogenesis. Mice deficient in GNMT develop liver steatosis that progresses to HCC [28,29,32–34]. These observations, and the potential far-reaching actions of higher methyl donor availability, prompted our previous studies aimed at determining the impact

Division of Molecular Medicine, Department of Medicine, University of Minnesota, Minneapolis, MN, USA

*Corresponding author. Division of Molecular Medicine, Department of Medicine, University of Minnesota, MCB 5-142, 420 Washington Avenue SE, Minneapolis, MN, 55455, USA. E-mail: chughey@umn.edu (C.C. Hughey).

Received November 7, 2021 • Revision received January 10, 2022 • Accepted January 27, 2022 • Available online 2 February 2022

https://doi.org/10.1016/j.molmet.2022.101452

of GNMT deletion on liver oxidative metabolism. We showed that the increased liver SAM in GNMT-null mice was accompanied by decreased liver gluconeogenesis, citric acid cycle flux, and oxidative phosphorylation [28,29]. These metabolic impairments were observed in the presence of liver steatosis in 12-week-old GNMT-null mice and persisted to the development of HCC at 44 weeks of age [28,29]. Our previous work suggests that loss of GNMT promotes lipid accumulation in part via impaired liver oxidative metabolism.

Given that GNMT governs SAM homeostasis, we had previously hypothesized that excess SAM availability was responsible for the decreased glucose and mitochondrial nutrient fluxes in mice lacking GNMT [28,29]. However, a recent study reported that GNMT physically interacts with and increases the activity of succinate dehydrogenase [17]. Thus, the loss of GNMT may inhibit citric acid cycle flux, independent of the higher SAM. Here we test the SAM-dependent and SAM-independent dysregulation of liver oxidative metabolism upon loss of GNMT. GNMT-null mice and WT littermates were fed a control or methionine-restricted diet to prevent elevated SAM. A combination of static and dynamic phenotyping approaches including targeted metabolomics, mitochondrial respirometry, and $^{2}H/^{13}C$ metabolic flux analysis (MFA) were used to define *in vivo* nutrient metabolism across multiple metabolic pathways.

2. MATERIAL AND METHODS

2.1. Mice

All procedures were approved by the Institutional Animal Care and Use Committee at the University of Minnesota. Mice received Teklad Global 18% Protein Rodent Diet (2918, Madison, WI) upon weaning at 3 weeks of age until beginning dietary interventions at 6 weeks of age. The first set of experiments studied mice with a whole-body knockout (KO) of GNMT, and WT littermates [28–30] that were provided a control diet (CON; L-AA Defined Diet with Dextrose and 0.86% DL-Methionine, 510072, Dyets Inc., Bethlehem, PA) or methionine-restricted diet (MR; L-AA Defined Diet with Dextrose and 0.172% DL-Methionine, 510071). In separate experiments, WT and KO mice were fed a control diet (CON; Rodent Diet with 10 kcal% Fat and 1.97 mg/kg folic acid, D12450J, Research Diets Inc., New Brunswick, NJ) or a folic acid-supplemented diet (FS, 19.03 mg/kg folic acid, D20110401). In a third set of experiments, WT mice were provided a high-fat diet (HF; 60% kcal from fat, A19011107, Research Diets Inc.) or a HF diet deficient in serine and glycine (HF-SG, A20042901). Mice had ad libitum access to food and water and were housed with cellulose bedding (Cellu-nest™, Shepherd Specialty Papers, Watertown, TN) in a temperature- and humidity-controlled room on a 14/10-hour light/dark cycle. Experiments were completed in male mice on a C57BL/6J background at 12 weeks of age unless otherwise stated.

2.2. Body composition

Body composition was determined in 11-week-old mice using a EchoMRI-100™ Body Composition Analyzer (EchoMRI LLC, Houston, TX).

2.3. Surgical procedures

Jugular vein and carotid artery catheterization surgeries were performed as previously described [35] in 11-week-old mice for venous infusion and arterial sampling protocols. Mice were individually housed during a 7-day postoperative recovery period and were within 10% of their pre-surgical weight prior to completing the stable isotope infusion experiments.

2.4. Stable isotope infusions

Stable isotope infusion experiments were completed over a 7-hour period. Food and water were withdrawn during the first hour of the light cycle (between 6 and 7 am). Two hours into the fast, the exteriorized ends of both vascular catheters were connected to infusion syringes via a two-channel swivel. Mice were given a 1-hour acclimation period following connection to the swivel before obtaining 80 μl arterial blood sample for determining natural isotopic enrichment of plasma glucose. Venous infusions were performed, as previously described, in conscious, unrestrained mice [28,29,36]. Briefly, a bolus of $^{2}H_2O$ (99.9%)-saline solution was administered over a 25-minute period to enrich body water at 4.5%. Mice received [6,6-$^{2}H_2$]glucose (99%) as a primed (440 μmol/kg, solubilized in the $^{2}H_2O$-saline bolus), continuous (4.4 μmol/kg/minute) infusion. Two hours following the $^{2}H_2O$ bolus and [6,6-$^{2}H_2$]glucose prime, a primed (1.1 mmol/kg), continuous (0.055 mmol/kg/minute) infusion of [$^{13}C_3$]propionate (99%, sodium salt) was initiated. An arterial sample (100 μl) was obtained every 10 minutes between the 90 and 120 minute mark after initiating the [$^{13}C_3$]propionate bolus and stored at −80 °C for measuring glucose enrichment, insulin, and non-esterified fatty acids (NEFAs). Donor red blood cells were delivered to maintain hematocrit within 10% of baseline values. Mice were sacrificed via cervical dislocation, and tissues were rapidly excised, freeze-clamped, and stored at −80 °C.

2.5. $^{2}H/^{13}C$ metabolic flux analysis

$^{2}H/^{13}C$ metabolic flux analysis was completed as previously outlined [28,29,36,37] with minor modifications. Briefly, three derivatives of plasma glucose (methyloxime pentapropionate, aldonitrile pentapropionate, and di-*O*-isopropylidene propionate) were prepared. Gas chromatography-mass spectrometry protocols were performed using a Thermo Scientific ISQ 7000 GC–MS system coupled to a Thermo Scientific TRACE 1310 gas chromatograph (Waltham, MA) with an HP-5 ms capillary column (19091S-433, Agilent Technologies Inc., Santa Clara, CA). Mass isotopomer distributions were obtained for fragment ions: methyloxime, *m/z* 145–149; aldonitrile, *m/z* 173–178, 259–266, 284–291,370–379; and di-*O*-isopropylidene, *m/z* 301–314. Estimates of fluxes from each sample were repeated 50 times from random starting values. Goodness-of-fit was determined using a chi-square test ($p = 0.05$) with 34 degrees of freedom. Quantified fluxes for each mouse are the mean of values acquired from samples at 90, 100, and 110 minutes after initiating the [$^{13}C_3$]propionate bolus and normalized to liver weight.

2.6. Blood and plasma analyses

Blood glucose was determined using Contour® blood glucose meters (Ascensia Diabetes Care, Parsippany, NJ). Plasma NEFAs were measured using the Wako HR series NEFA-HR(2) assay (FUJIFILM Medical Systems USA, Lexington, MA). Plasma insulin was quantified using the Mercodia Ultrasensitive Mouse Insulin ELISA (10-1249-01, Winston Salem, NC).

2.7. Tissue metabolites

Seven-hour fasted, non-catheterized mice were sacrificed via cervical dislocation, and liver tissue was collected for metabolites analysis. Liver samples were sent to Human Metabolome Technologies America, Inc. (Boston, MA) for targeted and untargeted metabolite quantification as previously described [38–41]. Phospholipids, diacylglycerides, and triacylglycerides were measured as previously outlined [42]. Glycogen was determined as previously described [43].

2.8. Immunoblotting

Liver tissue homogenates were prepared as previously detailed [28,36]. Gel electrophoresis was completed using a NuPAGE 4%—12% Bis-Tris gel (Invitrogen, Carlsbad, CA) and proteins transferred to a PVDF membrane. Primary antibodies used were as follows: mitochondrial encoded cytochrome c oxidase I (MT—CO1, ab14705), NADH dehydrogenase (ubiquinone) iron-sulfur protein 4 (NDUFS4, ab139178), and Total OXPHOS Rodent WB Antibody Cocktail (ab110413) from Abcam (Cambridge, MA). Acetyl-CoA carboxylase (ACC, 3662S), albumin (4929S), cytochrome c oxidase subunit 4 (COVIX, 4850S), DNA methyltransferase 1 (DNMT1, 5032S), phospho-glycogen synthase Ser641 (p-GS, 3891S), fatty acid synthase (FASN, 3180S), 3-hydroxymethylglutaryl-CoA synthase 2 (HMGCS2, 20940S), methylenetetrahydrofolate reductase (MTHFR, 25164S), phosphoglycerate dehydrogenase (PHGDH, 13428), stearoyl-CoA desaturase 1 (SCD1, 2794S), and succinate dehydrogenase subunit A (SDHA, 5839S) were from Cell Signaling Technology (Danvers, MA). β-hydroxybutyrate dehydrogenase (BDH1, 15417-1-AP), Glucose-6-phosphatase (G6PC, 22169-1-AP), GNMT (18790-1-AP), glycogen phosphorylase (PYGL, 15851-1-AP), total glycogen synthase (GS, 22371-1-AP), medium-chain acyl-CoA dehydrogenase (ACADM, 55210-1-AP), mitochondrial encoded cytochrome c oxidase II (MT—CO2, 55070-1-AP), nicotinamide N-methyltransferase (NNMT, 15123-1-AP), protein arginine N-methyltransferase 6 (PRMT6, 15395-1-AP), and phosphoserine aminotransferase 1 (PSAT1, 10501-1-AP) were from Proteintech® (Rosemont, IL). PVDF membranes were treated with SuperSignal™ West Pico PLUS chemiluminescent substrate (34577, Thermo Scientific) following secondary antibody incubation. A ChemiDoc™ Imaging system (Bio-Rad) was used to image PVDF membranes. Total protein was evaluated using BLOT-FastStain (G-Bioscience, Geno Technology Inc., St. Louis, MO) and was used as a loading control. ImageJ software was used to determine densitometry measurements.

2.9. Alkaline phosphatase treatment

Liver tissue was homogenized in a buffer (pH 7.9) containing 100 mM NaCl, 50 mM Tris—HCl, 10 mM $MgCl_2$, 1 mM dithiothreitol, and HALT™ Protease Inhibitor Cocktail EDTA-Free (87785, Thermo Scientific). Liver homogenates were treated with or without alkaline phosphatase (20 U per 30 μg of protein, 11097075001, MilliporeSigma, St. Louis, MO) and incubated at 37 °C for 60 minutes. Immunoblotting protocols described above were followed to assess phosphorylated and unphosphorylated MTHFR.

2.10. Mitochondrial isolation, high-resolution respirometry, and enzyme activity

Liver mitochondria were isolated from ad libitum fed mice as previously described [44]. High-resolution respirometry was completed using an Oroboros Oxygraph-2k (Oroboros Instruments, Innsbruck, Austria). Experiments were performed at 37 °C in duplicate and 2 ml of MiR05 (0.5 mM EGTA, 3 mM $MgCl_2$—$6H_2O$, 20 mM taurine, 10 mM KH_2PO_4, 20 mM HEPES, 1 g/liter BSA, 60 mM potassium-lactobionate, 110 mM sucrose, pH 7.1, adjusted at 30 °C). State 2 oxygen flux was tested with NADH-linked substrates, pyruvate (5 mM), glutamate (10 mM), and malate (2 mM). State 3 oxygen consumption assessed by a 5 mM ADP addition. Carbonyl cyanide 4-(trifluoromethoxy)phenylhydrazone (FCCP) was titrated in 0.1 μM steps to quantify maximal electron transport system-mediated oxygen flux (ETS). Rotenone (0.5 μM) and antimycin A (2.5 μM) provided residual oxygen consumption. Respiration supported by N,N,N′,N′-Tetramethyl-p-phenylenediamine dihydrochloride (TMPD, 0.5 mM) and ascorbate (2 mM) and corrected for autooxidation (1 mM KCN) tested cytochrome c oxidase function. Liver citrate synthase activity was determined at 25 °C as previously described [45]. Liver succinate dehydrogenase activity was quantified using the Succinate Dehydrogenase Activity Assay Kit from Abcam (ab228560).

2.11. Statistical analyses

Student's t-test or two-way ANOVA were used to assess statistical differences ($p < 0.05$), followed by Tukey's post hoc tests using GraphPad Prism software (GraphPad Software LLC., San Diego, CA). Data are reported as mean ± SEM.

3. RESULTS

3.1. Methionine restriction prevents hepatomegaly and liver steatosis in KO mice

Both the loss of GNMT and dietary methionine restriction lowered body weight (Figure 1A) compared to WT mice fed a control diet. Liver weights of KO mice were higher compared to WT mice on both diets (Figure 1B). Dietary methionine restriction reduced liver weight in both genotypes compared to mice on the control diet (Figure 1B). Notably, liver weights of KO mice fed a methionine-restricted diet were comparable to those of WT mice on the control diet (Figure 1B). Similar results were observed for the liver weight-to-body weight ratio (Figure 1C).

The changes in liver weight were not accompanied by differences in albumin, a hepatocyte marker (Figure 1D). However, liver lipids were altered (Figure 1E—K). Total phospholipids were increased in WT and KO mice receiving the methionine-restricted diet (Figure 1E). Malonylcarnitine was ~8-fold higher in KO mice compared to WT mice fed the control diet (Figure 1G). This increase was completely abrogated by the methionine-restricted diet (Figure 1G). The increased liver triacylglycerides in KO mice on a control diet were prevented by dietary methionine restriction (Figure 1I). The triacylglyceride 16:1/16:0 ratio was higher in KO mice on the control diet (Figure 1J). The low methionine diet decreased both the triacylglyceride 16:1/16:0 and 18:1/18:0 ratios in WT and KO mice (Figure 1J and K). In agreement, the methionine-restricted diet reduced stearoyl-CoA desaturase 1 (SCD1) in both WT and KO mice (Figure 1L), eliminating the 4-fold increase in SCD1 protein in KO mice (compared to WT mice) that were maintained on the control diet. Restricting methionine also modestly diminished acetyl-CoA carboxylase (ACC) and fatty acid synthase (FASN) protein (Figure 1L). These results show that dietary methionine restriction limits lipid accretion and lowers the expression of enzymes involved in lipid synthesis.

3.2. Methionine restriction enhances gluconeogenesis in both WT and KO mice

Our previous work suggested that liver steatosis in KO mice is driven by citric acid cycle intermediates being diverted away from glucose formation to lipogenesis [28]. Here we show that the suppression of endogenous glucose production in KO mice on a control diet was prevented by dietary methionine restriction (Figure 2A and B). Similarly, the decline in glycogenolysis (Figure 2A and C) and total gluconeogenesis (Figure 2A and D) in KO mice receiving the control diet was attenuated by dietary methionine restriction. The restoration of total gluconeogenesis in KO mice was linked to increased flux from phosphoenolpyruvate (Figure 2A, E, and F). Interestingly, a methionine-restricted diet increased gluconeogenesis from glycerol and phosphoenolpyruvate in WT mice compared to their control diet counterparts (Figure 2D—F). These data suggest that a methionine-restricted diet not only prevents the decreased gluconeogenesis in KO mice but enhances gluconeogenic flux independent of genotype.

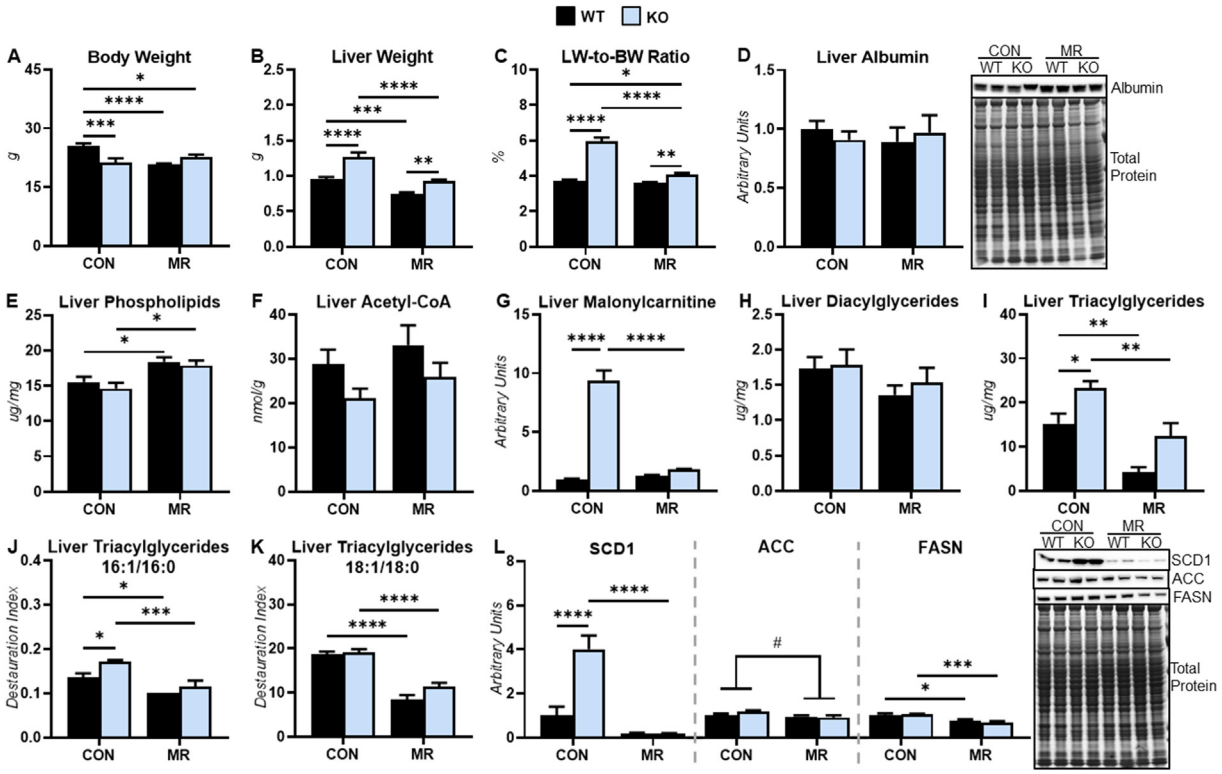

Figure 1: Dietary methionine restriction lowers liver pathology and triglyceride deposition in GNMT-null mice. (A) Body weight, **(B)** liver weight, and **(C)** liver-to-body weight ratio in fasted mice (n = 6–8 per group). **(D)** Liver albumin as determined by immunoblotting with a representative immunoblot (n = 7–8 per group). **(E)** Phospholipids (μg/mg liver), **(F)** acetyl-CoA (nmol/g liver), **(G)** malonylcarnitine (arbitrary units), **(H)** diacylglycerides (μg/mg liver) and **(I)** triacylglycerides (μg/mg liver), **(J)** triacylglyceride 16:1/16:0, and **(K)** triglyceride 18:1/18:0 in livers of fasted mice (n = 7–8 per group). **(L)** Liver stearoyl-CoA desaturase 1 (SCD1), acetyl-CoA carboxylase (ACC), and fatty acid synthase (FASN) as determined by immunoblotting with a representative immunoblot (n = 6–8 per group). Data are presented as mean ± SEM. *p < 0.05. **p < 0.01. ***p < 0.001. ****p < 0.0001. Main effect of diet, #p < 0.05.

Metabolite concentrations and expression of molecular regulators of glucose metabolism were assessed to support the interpretation of glucose fluxes. The decline in blood glucose levels in KO mice fed a control diet was attenuated in KO mice fed the methionine-restricted diet (Figure 2G). Liver glucose-6-phosphatase (G6PC) was decreased in KO mice on a methionine-restricted diet compared to KO mice on the control diet (Figure 2H and I). Glucose-6-phosphate, an immediate glucose precursor, was decreased in KO mice on both diets (Figure 2J). The accumulation of glycogen in KO mice on a control diet was abrogated by dietary methionine restriction (Figure 2K); however, a decline in glucose-1-phosphate in KO mice did not change in response to the dietary intervention (Figure 2L). PYGL protein and the p-GS/GS ratio were comparable between groups (Figure 2M–O). The methionine-restricted diet increased gluconeogenic precursors in the livers of KO mice (Figure 2P–T). Intermediates of gluconeogenesis from phosphoenolpyruvate trended higher in WT mice receiving a methionine-restricted diet compared to WT mice fed the control diet (Figure 2R–T). Our findings that dietary methionine restriction restored glycogen levels and increased gluconeogenic intermediates in KO mice are consistent with the normalized glycogenolysis and higher gluconeogenesis in KO mice fed a methionine-restricted diet.

3.3. Methionine restriction increases cataplerosis independent of citric acid cycle fluxes

Given that gluconeogenesis is often influenced by mitochondrial metabolism, citric acid cycle and related fluxes were quantified (Figure 3A). Flux of phosphoenolpyruvate to pyruvate (V_{PK+ME}) was higher in WT but not in KO mice fed a low methionine diet (Figure 3B). The flux of unlabeled lactate to pyruvate (V_{LDH}) was lower in KO mice compared to WT mice receiving a control diet (Figure 3C). Dietary methionine restriction increased V_{LDH} in both genotypes (Figure 3C). Anaplerosis from propionyl-CoA to succinyl-CoA (V_{PCC}) was diminished in KO mice on a control diet (Figure 3D). Anaplerotic flux from pyruvate to oxaloacetate (V_{PC}) and V_{PCC} were elevated in both genotypes fed a methionine-restricted diet (Figure 3D and E). Similarly, cataplerotic flux (V_{PCK}, flux from oxaloacetate to phosphoenolpyruvate) increased in mice fed a methionine-restricted diet (Figure 3F). Citric acid cycle fluxes (V_{CS} and V_{SDH}) were reduced in KO mice compared to WT mice on both diets (Figure 3G and H).

Citric acid cycle-related enzyme activity and metabolites were determined in conjunction with fluxes (Figure 3I–T). Maximal citrate synthase activity was decreased by dietary methionine restriction in both genotypes (Figure 3I). The impaired V_{CS} and V_{SDH} fluxes in control diet-fed KO mice were accompanied by a buildup of citrate (Figure 3J) and α-ketoglutarate (Figure 3K) as well as a trend toward decreased fumarate (Figure 3M), fumarate-to-succinate ratio (Figure 3N), and maximal succinate dehydrogenase activity (Figure 3O) that were normalized by dietary methionine restriction. KO mice showed higher levels of anaplerotic substrates on both diets (Figure 3Q–T). Our metabolomic, enzymatic, and nutrient flux results suggest that the methionine-restricted diet promotes nutrient efflux from the citric acid cycle towards glucose production; however, it does not completely resolve citric acid cycle impairments in KO mice.

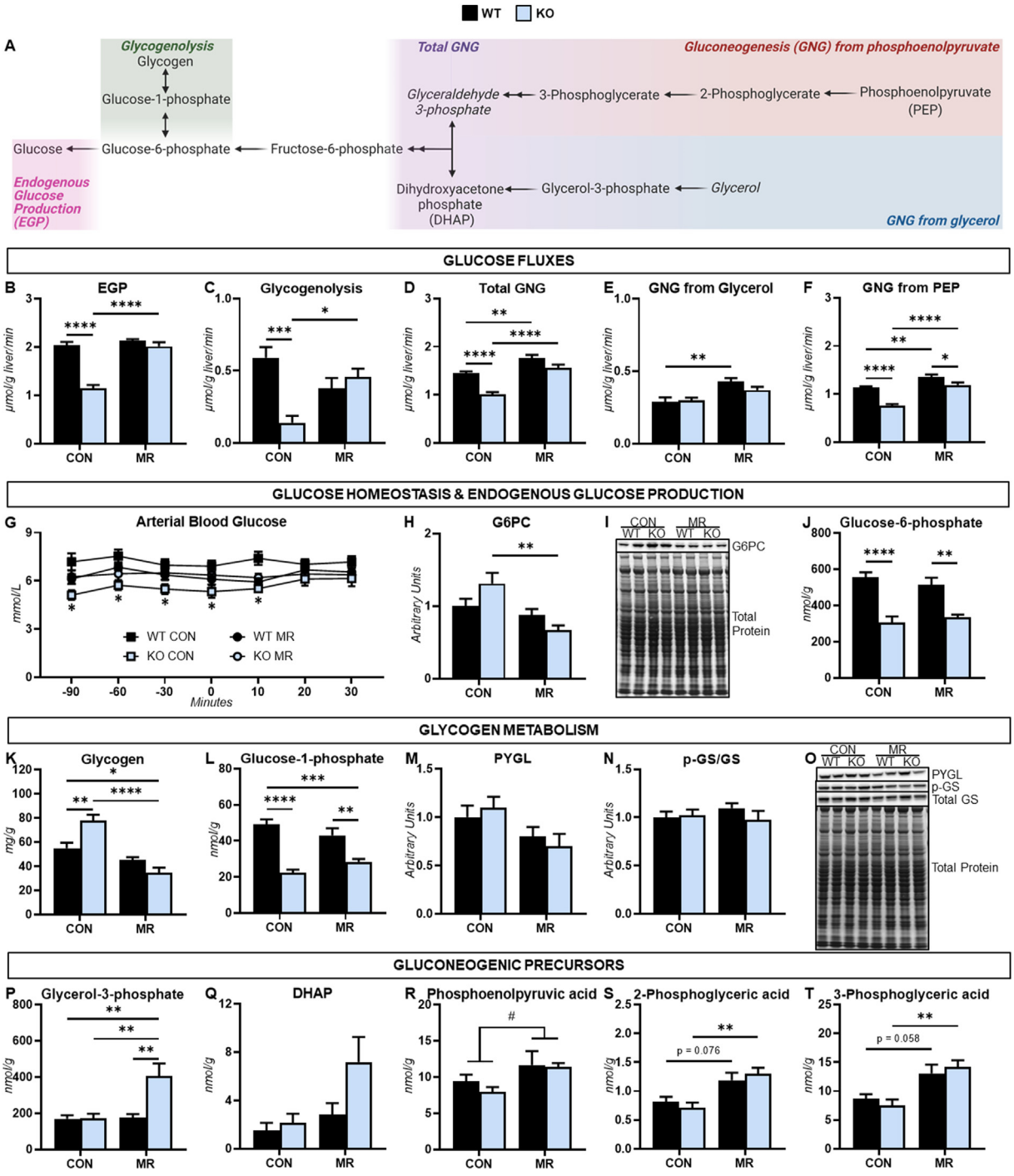

Figure 2: Methionine restriction minimizes dysregulated glucose metabolism in glycine N-methyltransferase knockout mice. (A) A schematic representation of select metabolites and metabolic fluxes from $^{2}H/^{13}C$ metabolic flux analysis in fasted glycine N-methyltransferase (GNMT)-null (KO) mice and wild-type (WT) littermates receiving a control (CON) and methionine-restricted (MR) diet. Italicized metabolites (glycerol and glyceraldehyde-3-phosphate) were not determined. **(B)** Endogenous glucose production (EGP), **(C)** glycogenolysis, **(D)** total gluconeogenesis (GNG), **(E)** GNG sourced from glycerol (hexose units), and **(F)** GNG flux sourced from phosphoenolpyruvate (PEP) (hexose units) expressed per liver weight (µmol/g/min; n = 5–10 per group). **(G)** A time course of blood glucose concentration before and during arterial sampling for $^{2}H/^{13}C$ metabolic flux analysis (n = 6–10 per group). **(H)** Liver glucose-6-phosphatase (G6PC) as determined by immunoblotting with a **(I)** representative immunoblot (n = 7–8 per group). **(J)** Liver glucose-6-phosphate (nmol/g), **(K)** glycogen (mg/g), and **(L)** glucose-1-phosphate (nmol/g) (n = 7–8 per group). **(M)** Liver glycogen phosphorylase (PYGL) and **(N)** phospho-glycogen synthase-to-total glycogen synthase ratio (p-GS/GS) as determined by immunoblotting with a **(O)** representative immunoblot (n = 7–8 per group). **(P)** Liver glycerol-3-phosphate, **(Q)** dihydroxyacetone phosphate (DHAP), **(R)** phosphoenolpyruvic acid, **(S)** 2-phosphoglyceric acid, and **(T)** 3-phosphoglyceric acid (nmol/g; n = 4–8 per group). Data are presented as mean ± SEM. *p < 0.05. **p < 0.01. ***p < 0.001. ****p < 0.0001. Main effect of diet, #p < 0.05.

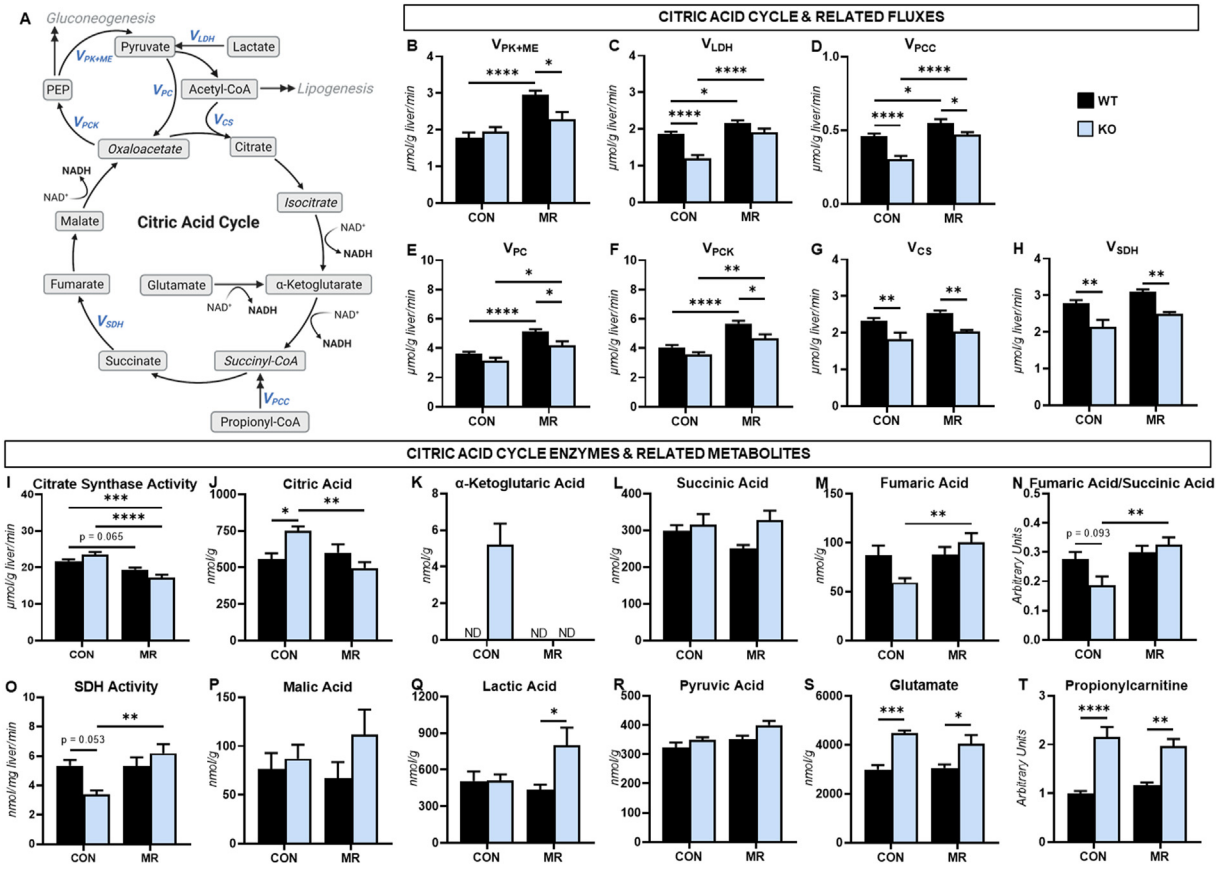

Figure 3: Methionine restriction increases citric acid cycle anaplerotic and cataplerotic fluxes. (A) A schematic representation of select metabolites and metabolic fluxes (highlighted in blue) from $^{2}H/^{13}C$ metabolic flux analysis associated with the citric acid cycle. Metabolic fluxes normalized to liver weight (μmol/g liver/min) were determined in wild-type (WT) and glycine N-methyltransferase knockout (KO) mice receiving a control (CON) or methionine-restricted (MR) diet for **(B)** the contribution of pyruvate kinase and malic enzyme to flux generating pyruvate (V_{PK+ME}), **(C)** flux of unlabeled lactate to pyruvate (V_{LDH}), **(D)** anaplerotic flux from propionyl-CoA to succinyl-CoA (V_{PCC}), **(E)** anaplerotic flux from pyruvate to oxaloacetate (V_{PC}), **(F)** cataplerotic flux of oxaloacetate to phosphoenolpyruvate (PEP) (V_{PCK}), **(G)** flux from oxaloacetate and acetyl-CoA to citrate (V_{CS}), and **(H)** flux from succinyl-CoA to oxaloacetate (V_{SDH}) (n = 6–10 per group). **(I)** Liver citrate synthase activity (μmol/g liver/min; n = 7–8 per group). **(J)** Liver citric acid (nmol/g), **(K)** α-ketoglutaric acid (nmol/g), **(L)** succinic acid (nmol/g), **(M)** fumaric acid (nmol/g), **(N)** fumaric-to-succinic acid ratio (arbitrary units; n = 7–8 per group). **(O)** Liver succinate dehydrogenase activity (nmol/g liver/min; n = 7–8 per group). **(P)** Liver malic acid, **(Q)** lactic acid, **(R)** pyruvic acid, **(S)** glutamate (nmol/g; n = 7–8 per group), and **(T)** propionylcarnitine (arbitrary units; n = 7–8 per group). Data are presented as mean ± SEM. ND = not detected. *p < 0.05. **p < 0.01. ***p < 0.001. ****p < 0.0001.

3.4. Methionine restriction minimizes dysregulated NAD$^+$ metabolism in livers of KO mice

Reactions within the citric acid cycle are dependent on NAD$^+$ availability and redox (NAD$^+$/NADH) homeostasis (Figure 3R). Given this, the relationship between the methionine cycle and NAD$^+$ metabolism was evaluated. Loss of GNMT in mice receiving the control diet increased liver methionine (Figure 4A and B), SAM (Figure 4C), and SAH (Figure 4D) approximately 7-, 74-, and 5-fold, respectively. Dietary methionine restriction completely blocked the accumulation in these metabolites (Figure 4B–D) and increased adenosine in KO mice (Figure 4E). In KO mice fed a control diet, there was an increase in other SAM-dependent methyltransferases (Figure 4F). Notably, methionine restriction prevented the 4-fold increase in nicotinamide N-methyltransferase (NNMT) in KO mice fed a control diet (Figure 4F). NNMT connects the methionine cycle to redox homeostasis via its actions in transferring a methyl group from SAM to nicotinamide generating SAH and 1-methylnicotinamide, which depletes the substrate for NAD$^+$ salvage (Figure 4A). In both genotypes, mice fed a methionine-restricted diet showed higher nicotinamide (Figure 4G). Despite normalized NNMT expression, 1-methylnicotinamide remained elevated in KO mice (Figure 4H). N^1-methyl-4-pyridone-5-carboxamide (4PY), a product of further 1-methylnicotinamide metabolism that is directed away from NAD$^+$ synthesis, was higher in KO mice fed a control diet (Figure 4I). The decline in nicotinamide mononucleotide (NMN, a direct NAD$^+$ precursor) in control diet-fed KO mice was mitigated by the low methionine diet (Figure 4J). Moreover, the decreased NAD$^+$ in livers of KO mice was prevented by the dietary intervention (Figure 4K). This was associated with the restoration of NADH, the NAD$^+$/NADH ratio, and NADP$^+$ in livers of KO mice fed the methionine-restricted diet (Figure 4L–N). These data indicate that dietary methionine restriction restores NAD$^+$ salvage in KO mice in part by lowering SAM and NNMT.

3.5. Methionine restriction prevents cytochrome c oxidase dysfunction in livers of KO mice

Mitochondrial oxidative phosphorylation was assessed to further test the impact of GNMT deletion and dietary methionine restriction on liver oxidative metabolism (Figure 5). The low methionine diet increased liver NDUFS4 protein in WT and KO mice (Figure 5A). Loss of GNMT reduced cytochrome c oxidase subunit protein (COXIV) compared to WT mice on a control diet (Figure 5A). Restricting dietary methionine led to higher cytochrome c oxidase subunit protein (COXIV, MT–CO1, and

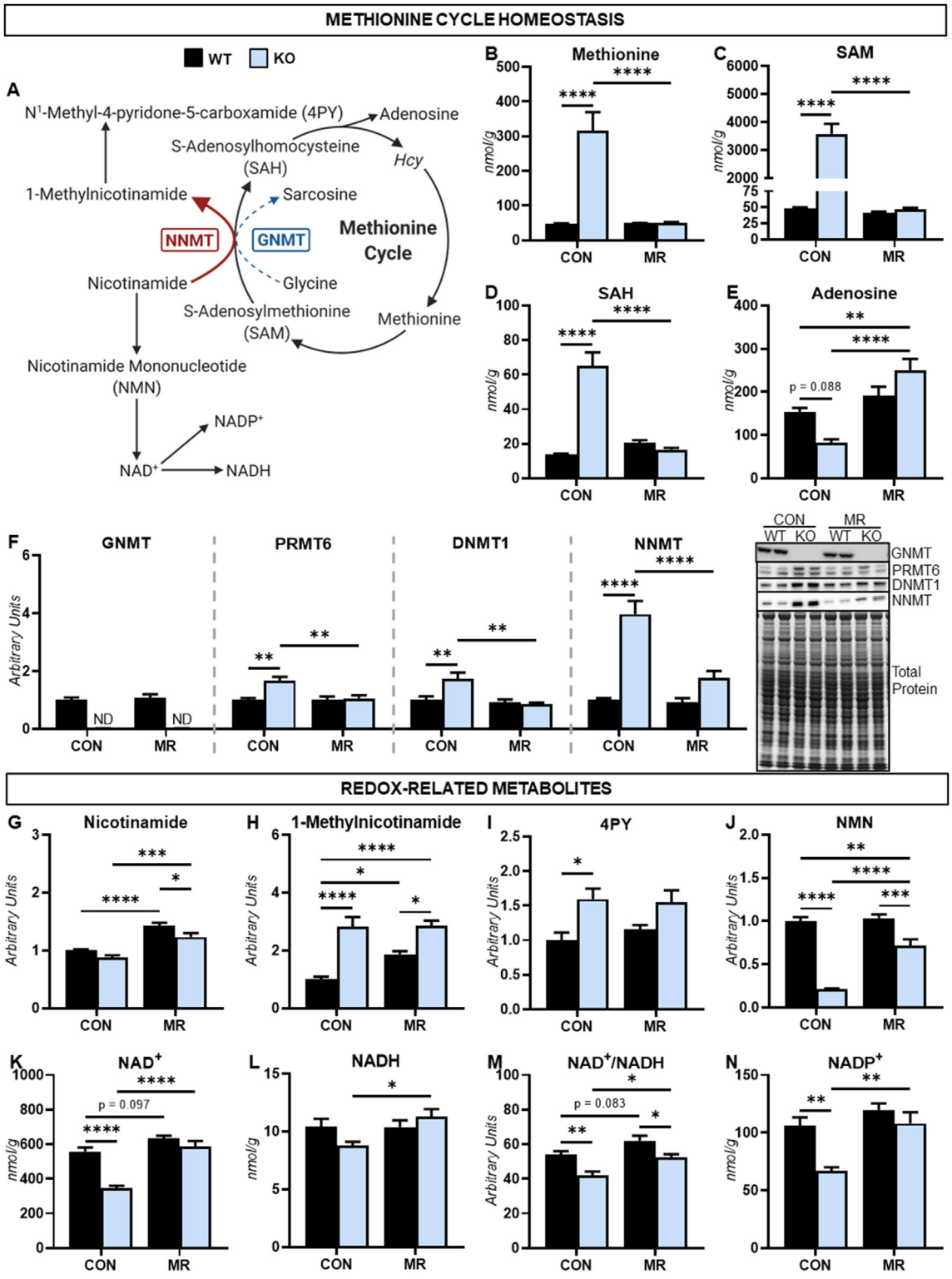

Figure 4: Methionine restriction lessens disruptions in NAD$^+$ homeostasis in livers of glycine N-methyltransferase knockout mice. (A) A schematic representation of select metabolites and enzymes integrating the methionine cycle with NAD$^+$ metabolism. The blue dash line indicates loss of glycine N-methyltransferase (GNMT). The thick red line indicates increased nicotinamide N-methyltransferase (NNMT) action. Italicized metabolites (Hcy, homocysteine) were not determined. **(B)** Liver methionine, **(C)** s-adenosylmethionine (SAM), **(D)** s-adenosylhomocysteine (SAH), and **(E)** adenosine in GNMT knockout (KO) and wild-type (WT) mice receiving a control (CON) and methionine-restricted (MR) diet (nmol/g; n = 7–8 per group). **(F)** Liver GNMT, protein arginine N-methyltransferase 6 (PRMT6), DNA methyltransferase 1 (DNMT1), and NNMT as determined by immunoblotting with a representative immunoblot (arbitrary units; n = 6–8 per group). **(G)** Liver nicotinamide, **(H)** 1-methylnicotinamide, **(I)** N^1-methyl-4-pyridone-5-carboxamide (4PY), **(J)** nicotinamide mononucleotide (NMN), **(K)** NAD$^+$, **(L)** NADH, **(M)** NAD$^+$-to-NADH ratio, and **(N)** NADP$^+$ (nmol/g or arbitrary units; n = 7–8 per group). Data are presented as mean ± SEM. *p < 0.05. **p < 0.01. ***p < 0.001. ****p < 0.0001.

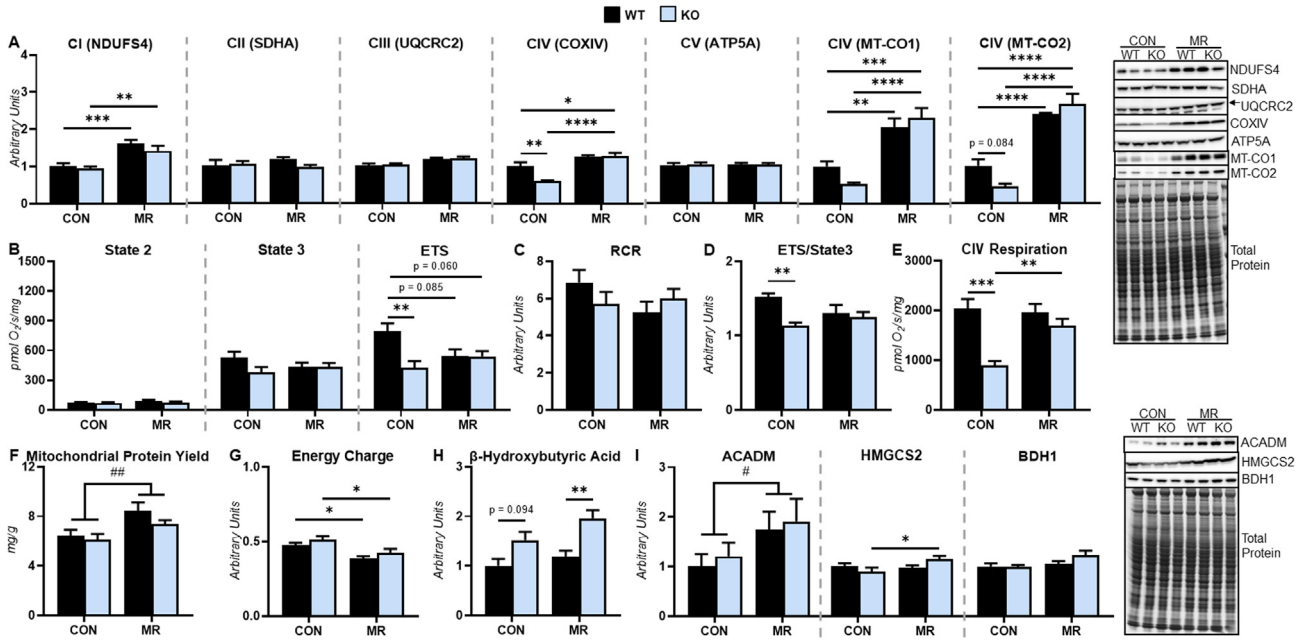

Figure 5: Dietary methionine restriction restores cytochrome c oxidase function. (A) Liver mitochondrial proteins (NDUFS4, SDHA, UQCRC2, COXIV, ATP5A, MT−CO1, and MT−CO2) in wild-type (WT) and glycine N-methyltransferase knockout (KO) mice fed a control (CON) or methionine-restricted (MR) diet as determined by immunoblotting with a representative immunoblot (arbitrary units; n = 7−8 per group). **(B)** Isolated liver mitochondria oxygen consumption rates normalized to mitochondrial protein (n = 5−6 per group; pmol O_2/s/mg). **(C)** Respiratory control ratio (RCR) and **(D)** ETS/State3 (n = 5−6 per group). **(E)** Cytochrome c oxidase (CIV) oxygen flux normalized to mitochondrial protein (n = 5−6 per group; pmol O_2/s/mg). **(F)** Mitochondrial protein per liver weight (mg/g). **(G)** Liver energy charge (energy charge = ([ATP] + 0.5*[ADP])/([ATP]+[ADP]+[AMP]) and **(H)** β-hydroxybutyric acid (arbitrary units; n = 8 per group). **(I)** Liver ACADM, HMGCS2, and BDH1 as determined by immunoblotting with a representative immunoblot (arbitrary units; n = 7−8 per group). Data are presented as mean ± SEM. *p < 0.05. **p < 0.01. ***p < 0.001. ****p < 0.0001. Main effect of diet, #p < 0.05, ##p < 0.01.

MT−CO2) in both genotypes (Figure 5A). State 2 and state 3 respiration rates supported by NADH-linked substrates were comparable between groups (Figure 5B). Maximal electron transport (ETS) with NADH-linked substrates was lower in KO mice compared to WT mice on a control diet (Figure 5B). The respiratory control ratio was comparable between groups (Figure 5C), however, ETS reserve capacity (ETS/State 3) was decreased in KO mice compared to WT mice on a control diet (Figure 5D). Cytochrome c oxidase respiratory function was decreased 2-fold in KO mice fed a control diet (Figure 5E). Dietary methionine restriction abrogated the decline in cytochrome c oxidase-mediated respiration (Figure 5E). Mitochondrial protein yield during the isolation protocols was higher from livers of mice fed the methionine-restricted diet (Figure 5F). Liver energy charge was reduced in response to dietary methionine restriction (Figure 5G). Liver β-hydroxybutyrate was higher in livers of KO mice receiving the methionine-restricted diet (Figure 5H). Liver medium chain acyl-CoA dehydrogenase (ACADM) protein was elevated in response to dietary methionine restriction. Mitochondrial 3-hydroxymethylglutaryl-CoA synthase (HMGCS2) protein was elevated in KO mice fed the methionine-restricted diet compared to KO mice fed the control diet (Figure 5I). These results indicate that loss of GNMT and methionine restriction have a pronounced impact on oxidative phosphorylation homeostasis.

3.6. Methionine restriction alleviates interruptions across one-carbon metabolism in KO mice

Previous work identified that GNMT deletion decreases tissue folate retention and impairs folate cycle function as indicated by lower nucleotide synthesis [46,47]. In agreement, our results showed markedly lower 5-methyltetrahydrofolate (5-MeTHF; Figure 6A and B), a prominent form of folate that functionally connects the methionine and folate cycles by donating a one-carbon group to homocysteine to form methionine and tetrahydrofolate [48]. Dietary methionine restriction increased 5-MeTHF tissue content in livers of both control and KO mice, restoring its levels in livers of KO mice to levels observed in livers of WT mice fed a control diet (Figure 6B). In addition, the decline in adenine nucleotide levels in KO mice on a control diet was prevented by a methionine-restricted diet (Figure 6C). Methylenetetrahydrofolate reductase (MTHFR), the enzyme that generates 5-MeTHF [49], was ~3-fold higher in livers of control diet-fed KO mice, and this increase was attenuated in KO mice receiving the methionine-restricted diet (Figure 6D). Notably, a large fraction of the MTHFR pool was phosphorylated (Figure 6E). SAM inhibits MTHFR activity through both allosteric and covalent modification (phosphorylation) mechanisms [50,51]. Thus, the increased MTHFR in KO mice proves insufficient to rescue 5-MeTHF synthesis or dysregulated folate and methionine cycle connectivity.

Folate cycle function is dependent on multiple one-carbon donors including serine, glycine, and sarcosine. The low methionine diet increased liver phosphoglycerate dehydrogenase (PHGDH) and phosphoserine aminotransferase 1 (PSAT1) in both WT and KO mice (Figure 6F). This was associated with a 56% and a 37% rise in concentrations of one-carbon donors serine and glycine, respectively, in WT mice (Figure 6G and H). KO mice fed the methionine-restricted diet showed higher glycine (Figure 6H). The one-carbon donor choline was comparable between groups (Figure 6I); however, its product, betaine, was elevated 15-fold in KO mice fed a control diet (Figure 6J). This magnitude increase was lowered to 5-fold on a methionine-restricted diet (Figure 6J). Dimethylglycine and sarcosine were increased in KO mice on the methionine-restricted diet (Figure 6K and L). Thus, dietary

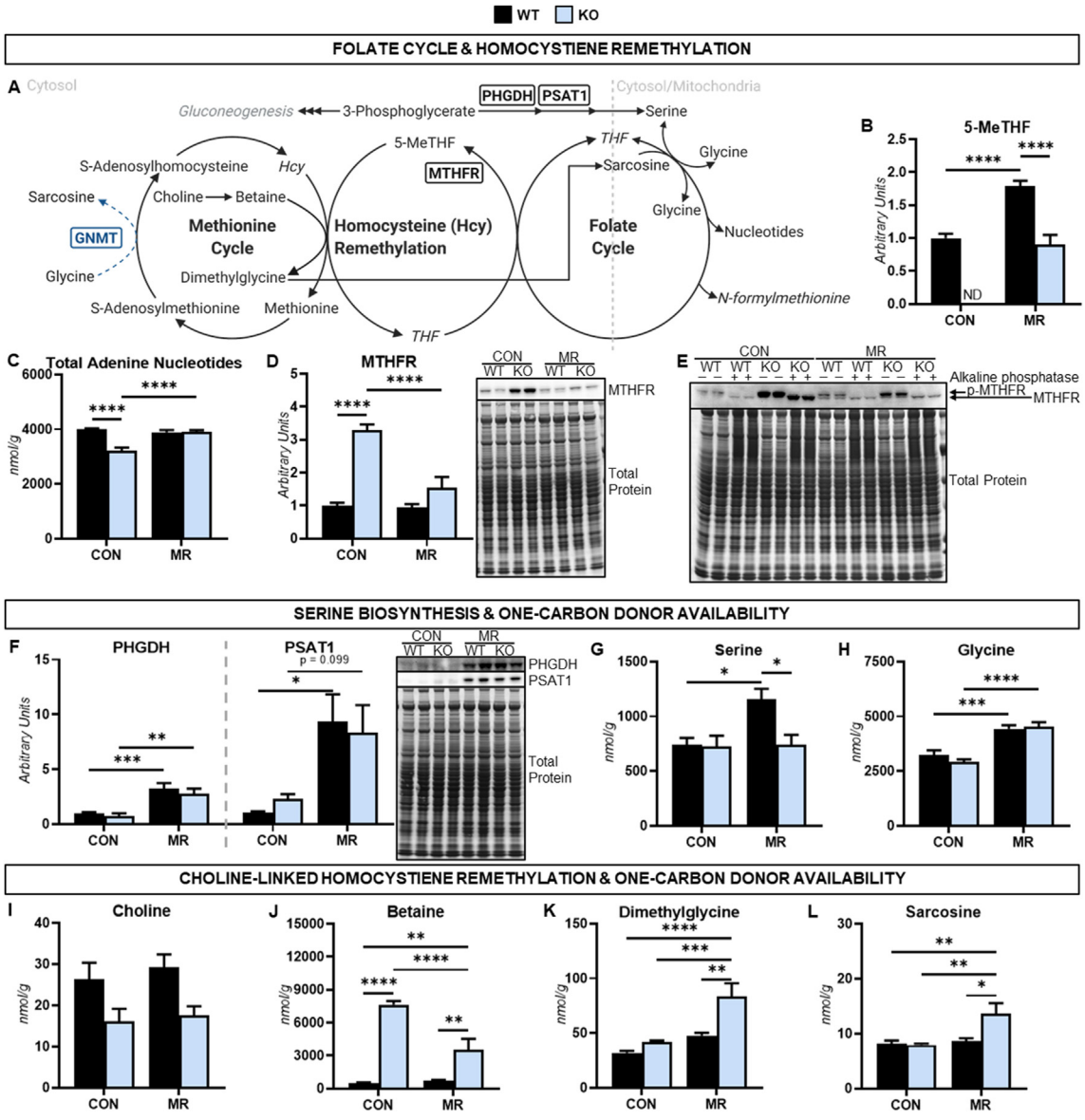

Figure 6: Dietary methionine restriction restores connectivity between folate and methionine cycles and increases one-carbon donor availability. (A) A schematic representation of select metabolites and reactions related to one-carbon metabolism. The blue dash line indicates loss of glycine N-methyltransferase (GNMT). Italicized metabolites (Hcy, homocysteine; N-formylmethionine; THF, tetrahydrofolate) were not measured. **(B)** Liver 5-methyltetrahydrofolate (5-MeTHF) and **(C)** total adenine nucleotides (nmol/g; n = 7–8 per group). **(D)** Liver methylenetetrahydrofolate reductase (MTHFR) as determined by immunoblotting with a representative immunoblot in GNMT knockout (KO) and wild-type (WT) littermates on a control (CON) and methionine-restricted (MR) diet (arbitrary units; n = 6–8 per group). **(E)** Representative image of phospho-MTHFR and unphosphorylated MTHFR as determined by immunoblotting. **(F)** Liver phosphoglycerate dehydrogenase (PHGDH) and phosphoserine aminotransferase 1 (PSAT1) as determined by immunoblotting with a representative immunoblot (arbitrary units; n = 7–8 per group). **(G)** Liver serine and **(H)** glycine (nmol/g; n = 7–8 per group). **(I)** Liver choline, **(J)** betaine, **(K)** dimethylglycine, and **(L)** sarcosine (nmol/g; n = 6–8 per group). Data are presented as mean ± SEM. ND = not detected. *p < 0.05. **p < 0.01. ***p < 0.001. ****p < 0.0001.

methionine restriction lowers SAM but promotes synthesis and/or availability of multiple other one-carbon donors. This may aid in restoring folate cycle function and/or connectivity with the methionine cycle.

3.7. Folate and one-carbon donor availability governs liver mitochondrial and lipid homeostasis

The folate cycle has nuclear-, cytosolic-, and mitochondrial-localized reactions that transfer one-carbon units for nucleotide and/or N-formylmethionine synthesis [52]. Thus, altered folate cycle function and one-carbon donor availability may impact mitochondrial DNA synthesis/integrity, gene transcription, and/or protein translation. To test the role of dysregulated folate cycle function on mitochondrial homeostasis, WT and KO mice were provided with a control or folic acid-supplemented diet. Liver MTHFR remained elevated in KO mice receiving the folate-supplemented diet (Figure 7A); however, the additional dietary folic acid prevented the decline in liver mitochondrial encoded cytochrome c oxidase II (MT–CO2) protein (Figure 7B). These results indicate that perturbed folate cycle function may contribute to the impaired cytochrome c oxidase function in KO mice.

To assess the impact of one-carbon donor availability on mitochondrial and lipid metabolism, WT mice were fed a high-fat (HF) or HF diet

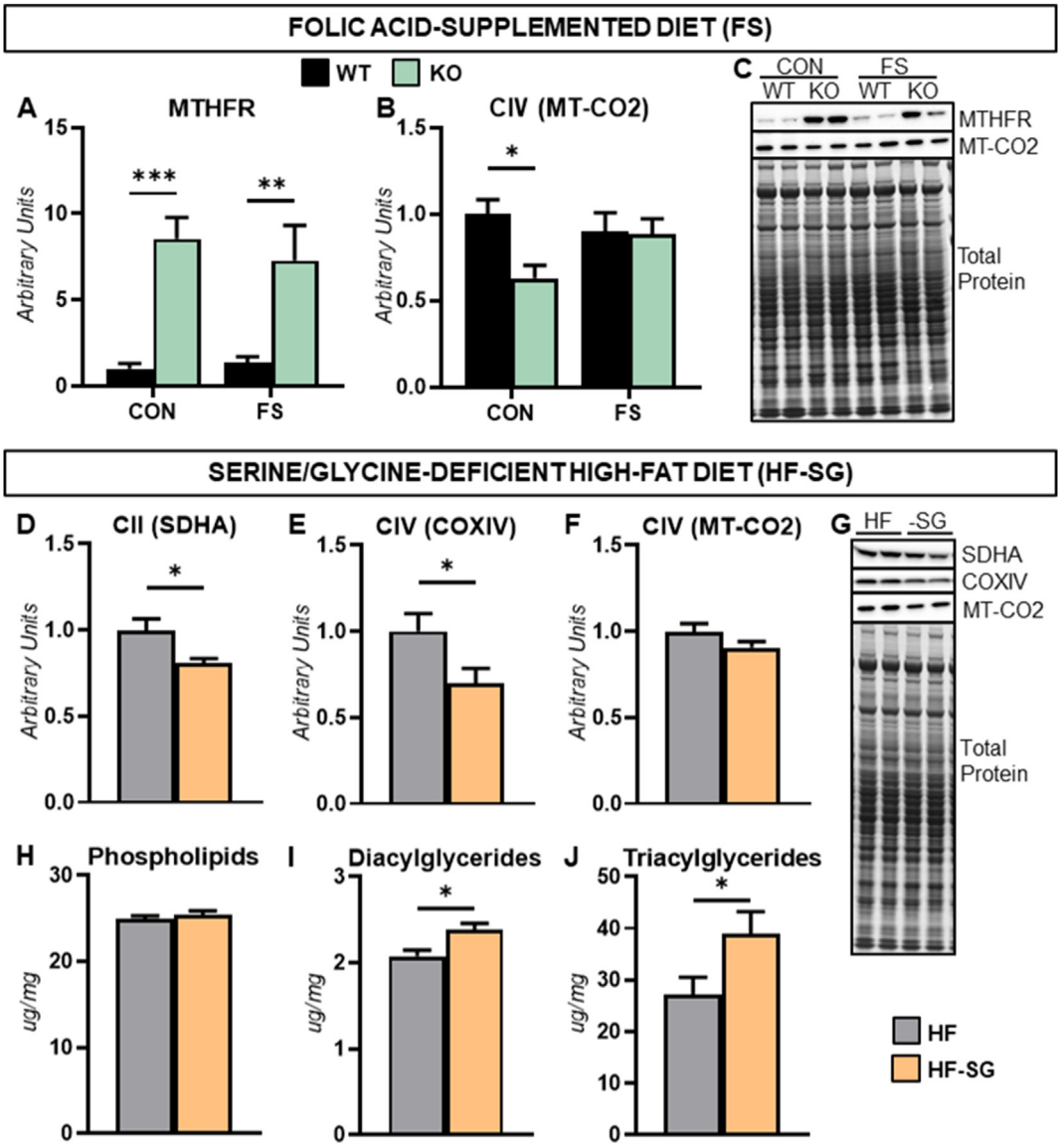

Figure 7: Folic acid and one-carbon donor availability regulate liver mitochondrial and lipid homeostasis. (A) Methylenetetrahydrofolate reductase (MTHFR) and **(B)** mitochondrially encoded cytochrome c oxidase II (MT−CO2) in livers of glycine N-methyltransferase (GNMT) knockout (KO) and wild-type (WT) mice fed a control (CON) or folate-supplemented (FS) as determined by immunoblotting with a **(C)** representative immunoblot (arbitrary units; n = 6−8 per group). **(D)** Liver succinate dehydrogenase subunit A (SDHA), **(E)** cytochrome c oxidase subunit 4 (COXIV), and **(F)** MT−CO2 in livers of WT mice receiving a high-fat diet (HF) and or a serine/glycine-deficient HF diet (-SG) as determined by immunoblotting with a **(G)** representative immunoblot (arbitrary units; n = 7−8 per group). **(H)** Liver phospholipids, **(I)** diacylglycerides, and **(J)** triacylglycerides (μg/mg; n = 7−8 per group). Data are presented as mean ± SEM. *p < 0.05. **p < 0.01. ***p < 0.001.

deficient in serine and glycine (HF-SG). Mice receiving the HF-SG diet showed decreased liver succinate dehydrogenase subunit A (SDHA) and COXIV (Figure 7D and E). Further, liver diacylglycerides and triacylglycerides were increased in mice fed the diet lacking serine and glycine (Figure 7I and J). These data suggest the increased one-carbon donor availability contributes to the mitochondrial and lipid phenotype observed in mice on the methionine-restricted diet.

3.8. Assessment of extrahepatic factors underlying liver lipid homeostasis

Like in fasted conditions, ad libitum fed KO mice receiving the control diet had lower body weights compared to WT mice (Figure 8A). A methionine-restricted diet decreased body weight in both genotypes compared to WT receiving a control diet (Figure 8A). Relative adiposity and lean mass were comparable between groups (Figure 8B and C), and plasma NEFAs were similar between groups (Figure 8D). Circulating insulin was decreased in KO mice on both diets and WT mice fed a methionine-restricted diet in relation to WT mice on the control diet (Figure 8E). These results suggest that the liver-specific actions of dietary methionine restriction are important in preventing liver steatosis in KO mice.

4. DISCUSSION

Studies in humans [15,17,21−26] and experimental models [15−20] have identified that decreased GNMT expression is common in NAFLD

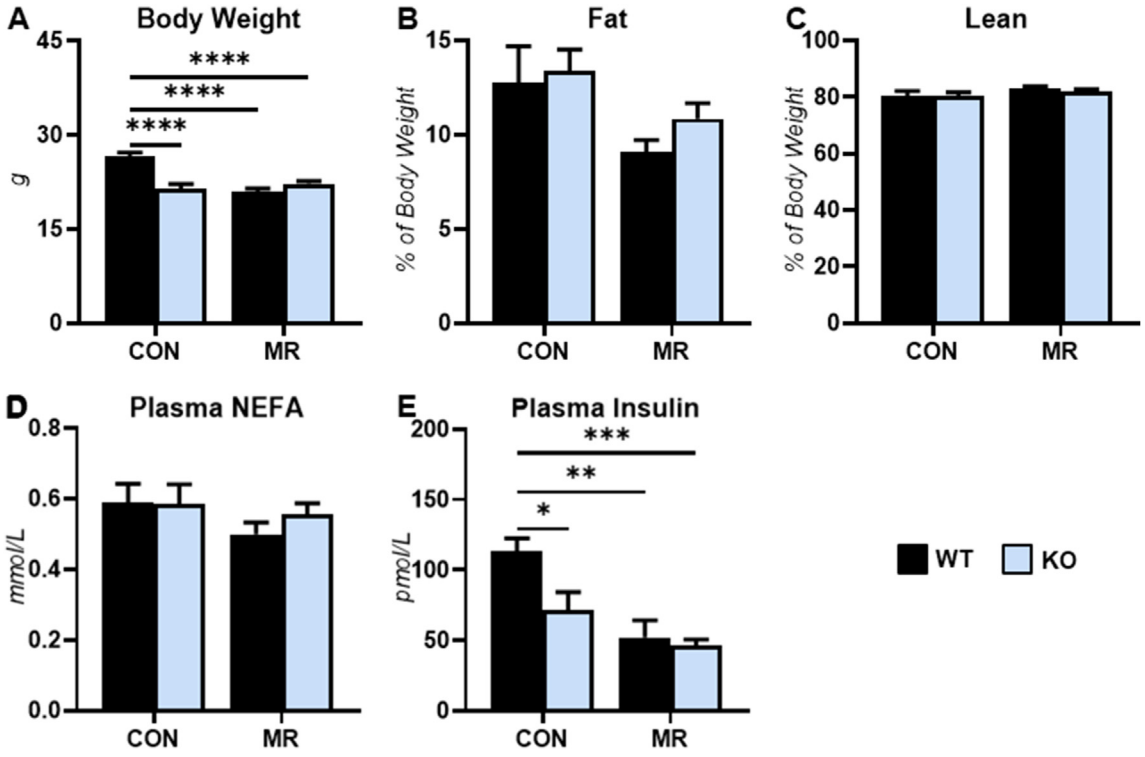

Figure 8: Dietary methionine restriction and extrahepatic metabolism. (A) Body weight, **(B)** fat mass as a percentage of body weight, and **(C)** lean mass as a percentage of body weight in ad libitum fed glycine N-methyltransferase (GNMT)-null (KO) mice and wild-type (WT) littermates receiving a control (CON) and methionine-restricted (MR) diet ($n = 10-13$ per group). **(D)** Fasting arterial non-esterified fatty acids ($n = 7-10$ per group). **(E)** Fasting arterial insulin (pmol/L; $n = 7-10$ per group). Data are presented as mean ± SEM. *$p < 0.05$. **$p < 0.01$. ***$p < 0.001$. ****$p < 0.0001$.

and NAFLD-associated HCC. A causal role for the loss of GNMT in NAFLD pathophysiology is supported by findings that GNMT-null mice develop liver steatosis that progresses to HCC [28,29,32–34]. The accumulation of liver lipids in GNMT-null mice is mediated in part by an imbalance between lipid accretion and disposal [28,29,53]. Prior research provides evidence that the increased SAM resulting from GNMT deletion underlies the metabolic remodeling [28,29,53]. However, recent experiments suggest that loss of GNMT may impair citric acid cycle enzyme activity independent of higher SAM [17]. The objective of this study was to define the SAM-dependent regulation of liver oxidative metabolism in GNMT KO mice.

4.1. Dietary methionine restriction and liver lipid homeostasis in KO mice

Consistent with prior work [21,28,32,53,54], KO mice displayed increased liver lipids. Martinez-Una et al. [53] found that the compensatory increase in phosphatidylethanolamine N-methyltransferase activity in GNMT-null mice contributes to liver steatosis. Specifically, the increased phosphatidylcholine generated from PEMT-mediated phosphatidylethanolamine methylation is diverted to triacylglyceride synthesis [53]. We previously identified that the elevated liver triacylglycerides in KO mice are associated with markers of increased de novo lipogenesis [28]. In this study, liver SCD1 and triacylglyceride desaturation were elevated in KO mice. SCD1 action generates long-chain monounsaturated fatty acids, which are preferentially committed to lipid deposition rather than oxidation [55,56]. To further define the mechanisms through which loss of GNMT promotes liver steatosis, mice were fed a methionine-restricted diet. Dietary methionine restriction prevented the accumulation of liver SAM in KO mice. This was accompanied by a pronounced reduction in SCD1 expression, triacylglyceride desaturation, and total triacylglycerides. Liver FASN and ACC, regulators of lipogenesis, were modestly lower in mice fed the methionine-restricted diet. These results suggest that the dietary methionine restriction reduces liver lipogenesis in KO mice. Future work that includes flux quantification is required to confirm lipogenesis is decreased.

4.2. Glucose formation in the livers of WT and KO mice fed a methionine-restricted diet

Fasting blood glucose was lower in KO mice fed a control diet. This was a consequence of decreased endogenous glucose production (EGP). Moreover, the decline in EGP is in part due to diminished glycogenolysis in KO mice. Liver glycogen was elevated in KO mice, which is consistent with impaired glycogenolysis. Novel findings in this study identified that dietary methionine restriction increased glycogenolysis and decreased liver glycogen in KO mice. This was associated with the restoration of EGP and circulating glucose levels. Few studies have investigated the mechanisms through which SAM and/or methionine cycle homeostasis regulate glycogen metabolism. We show that the key glycogen regulators glycogen phosphorylase and glycogen synthase were not influenced by loss of GNMT. Previous work reported that livers of GNMT-null mice exhibit a SAM-dependent impairment in the fusion of autophagic vacuoles with lysosomes [57]. In addition, GNMT-null mice have reduced expression of acid α-glucosidase, a lysosomal enzyme that hydrolyzes glycogen [31,58]. Thus, SAM-mediated attenuation of glycophagy may underly lower glycogenolysis in KO mice.

The impaired EGP in KO mice was also due to decreased gluconeogenesis from phosphoenolpyruvate. Our results indicate that the lower

gluconeogenesis was a consequence of dysregulated SAM homeostasis, as dietary methionine restriction increased gluconeogenic intermediates and restored gluconeogenic fluxes in KO mice. Interestingly, gluconeogenesis in WT mice receiving the methionine-restricted diet was higher compared to WT mice fed the control diet. This was surprising given that the dietary methionine restriction did not alter liver methionine and SAM levels in WT mice. Circulating insulin was lower in WT mice fed the low methionine diet compared to WT mice on the control diet. However, insulin action does not appear to be the sole factor for increased gluconeogenesis, as KO mice fed the methionine-restricted diet exhibited higher gluconeogenic flux compared to KO mice on the control diet despite comparable insulin levels. This suggests that glucoregulation by dietary methionine restriction is mediated partly by dynamic homeostasis of liver methionine cycle intermediates.

4.3. Citric acid cycle and related fluxes in WT and KO mice fed a methionine-restricted diet

The citric acid cycle is critical for terminal oxidation of nutrients. KO mice fed a control diet exhibited diminished anaplerosis (V_{PCC}) and provision of anaplerotic nutrients (V_{LDH}). Citric acid cycle fluxes (V_{CS} and V_{SDH}), the fumarate-to-succinate ratio, and SDH activity were all lower in KO mice fed a control diet. This was associated with the build-up of citric acid cycle and anaplerotic metabolites. These data showing disrupted citric acid cycle function in KO mice receiving a control diet are consistent with our prior work [28,29]. Our results also align with recent studies identifying that loss of GNMT reduces SDH activity [17]. Furthermore, the experiments presented here show that a methionine-restricted diet did not resolve the decreased *in vivo* citric acid cycle fluxes in KO mice. Conversely, the diminished fumarate-to-succinate ratio and SDH activity were rescued by dietary methionine restriction. It is currently unclear as to why the low methionine diet normalized tissue indices of SDH action but did not increase *in vivo* citric acid cycle fluxes. Our findings do suggest, however, that inhibition of *in vivo* citric acid cycle flux in KO mice is independent of the increased SAM.

Liver redox state was assessed to gain further insight into the dysregulated liver citric acid cycle flux in KO mice. Liver NAD^+ and the NAD^+-to-NADH ratio were lower in KO mice fed the control diet. The dysregulated redox state was accompanied by ~4-fold increase in NNMT. NNMT transfers a methyl group from SAM to nicotinamide forming 1-methylnicotinamide and SAH [59]. Both products were higher in KO mice, suggesting that NNMT action was increased. Given that nicotinamide is used in NAD^+ salvage, we previously speculated that the increased NNMT is a compensatory response to lower SAM that impedes NAD^+ salvage, decreases the NAD^+-to-NADH ratio, and thereby impairs citric acid cycle flux [29]. We found that dietary methionine restriction reduced NNMT and increased both NAD^+ and the NAD^+-to-NADH ratio in KO mice. These findings suggest that loss of GNMT impedes citric acid cycle flux via mechanisms that are independent of redox state. However, it should be noted that metabolite measurements were completed in whole liver tissue which may not fully reflect mitochondrial redox state.

Another conclusion arising from our data is that decreased citric acid cycle flux alone does not induce liver steatosis in KO mice. Dietary methionine restriction increased cataplerosis linked to gluconeogenesis (V_{PCK}) in WT and KO mice. Cytosolic phosphoenolpyruvate carboxykinase (PEPCK) is a key regulator of cataplerosis as evidenced by mice lacking liver PEPCK being characterized by impaired gluconeogenesis, cataplerosis, and citric acid cycle flux [60–62]. Moreover, chronic suppression of PEPCK activity promotes liver steatosis and HCC in experimental models [62–67]. Dietary methionine restriction may reduce steatosis in KO mice via the enhanced cataplerosis linked to gluconeogenesis. Under these conditions, cataplerosis could function as an outlet for excess nutrients and/or generate 3-phosphoglycerate for de novo serine synthesis (discussed in *Section 4.4*). Importantly, cataplerosis and gluconeogenesis are energetically costly as evidenced by the decline in liver energy state of mice fed the methionine-restricted diet. We also showed that dietary methionine restriction increased markers of β-oxidation and ketogenesis (ACADM, HMGCS2, β-hydroxybutyrate) in WT and/or KO mice. Independent work using ^{14}C-palmitate in liver homogenates has tested lipid oxidation in response to dietary methionine restriction [68,69]. Hasek et al. found that liver $^{14}CO_2 + {}^{14}$C-labeled acid soluble metabolites were increased in rats fed a methionine-restricted diet [68]. Malloy et al. did not observe higher $^{14}CO_2$ in rats receiving the low methionine diet, but liver β-hydroxybutyrate was elevated [69]. Together, these prior studies suggest β-oxidation and potentially ketogenesis are increased in response to dietary methionine restriction. In addition, the absence of changes in $^{14}CO_2$ alone is consistent with our findings that terminal oxidation in the citric acid cycle is not impacted by a low methionine diet. Thus, elevated β-oxidation contributes to both lipid catabolism and the energy demands of increased cataplerosis and gluconeogenesis in mice fed a methionine-restricted diet.

4.4. Dietary methionine restriction and oxidative phosphorylation in WT and KO mice

We previously showed that isolated hepatocyte routine respiration was lower in GNMT-null mice [28]. In this study we aimed to define site-specific impairments in respiratory chain function. Cytochrome c oxidase subunit protein was reduced in livers of KO mice, and cytochrome c oxidase function as assessed by oxygen flux was ~60% lower in KO mice. Both maximal electron transport (ETS) and reserve electron transport capacity (ETS/State 3) supported by NADH-linked substrates also decreased in KO mice. Together with our findings that SDH flux and activity are reduced, these results indicate multiple sites involved in oxidative phosphorylation are compromised by the loss of GNMT.

NADH:ubiquinone oxidoreductase and cytochrome c oxidase subunit proteins were higher in WT and KO mice fed a methionine-restricted diet. The dietary methionine restriction rescued cytochrome c oxidase dysfunction in KO mice but did not significantly influence respiratory flux in WT mice. In agreement, most [70–73] but not [74] all studies evaluating the impact of dietary methionine restriction on liver mitochondrial respiration report no change in WT mice. A methionine-restricted diet has been shown to reduce hepatic cytosolic and nuclear protein synthesis [75,76]. However, mitochondrial protein synthesis was not affected, leading the authors to conclude that hepatic mitochondrial protein integrity is prioritized during methionine restriction [75,76]. This selective maintenance of mitochondrial protein may explain the higher mitochondrial protein normalized to total tissue protein observed in our immunoblots, but comparable respiratory chain function normalized to mitochondrial protein. Furthermore, the compartmentation-specific impact of dietary methionine restriction on protein synthesis may contribute to greater liver lipid oxidation.

GNMT is part of a larger metabolic network termed one-carbon metabolism wherein one-carbon units are transferred within and between the methionine and folate cycles for biosynthetic purposes. Prior work has shown that total folate retention and folate cycle function are compromised by loss of GNMT [46,47]. Given that GNMT binds to 5-MeTHF [77], it was hypothesized that the lower folate in GNMT-null mice was due to reduced 5-MeTHF and that GNMT acts as a folate reservoir [46]. Here we demonstrate that 5-MeTHF is indeed depleted

in livers of KO mice; however, our data suggest that the excess SAM is at least partly responsible for the folate depletion, as dietary methionine restriction restored 5-MeTHF levels in KO mice. Our findings align with experiments showing SAM inhibits MTHFR activity [50,51]. To test the metabolic implications of lower folates and/or folate cycle dysregulation in livers lacking GNMT, mice were provided a folic acid-supplemented diet. Increasing dietary folic acid prevented the decline in MT—CO2 protein. Consistent with our findings, dietary folate deficiency decreases liver cytochrome c oxidase activity in rats [78]. In addition, dietary folate supplementation reduces liver steatosis in experimental models [79—81].

Serine and glycine are prominent one-carbon donors for folate cycle actions. Dietary methionine restriction increased liver serine and glycine in WT and KO mice. Independent of genotype, we show liver PHGDH and PSAT1 were higher in mice fed a methionine-restricted diet. These results provide evidence that restricting dietary methionine enhances de novo serine synthesis and one-carbon donor availability. The increased PHGDH and PSAT1 are among the most reproducible observations associated with dietary methionine restriction, making the expression of these enzymes a commonly used biomarker for a successful dietary intervention [82—90]. However, serine and glycine provision appear to have a more impactful role in NAFLD given that serine or glycine supplementation attenuates liver steatosis in rodents [91—94]. Here we demonstrate that dietary serine and glycine deficiency promote liver steatosis and decreases mitochondrial protein. Future research should test whether serine and glycine synthesis and/or availability mediate the mitochondrial adaptations to dietary methionine restriction.

In addition to testing the underlying actions of the methionine-restricted diet, further work is needed to define the mechanisms by which the higher SAM in KO mice impairs liver oxidative metabolism. Previous work has identified that loss of GNMT and/or increased SAM inhibit lipid degradation by autophagy [57], attenuate the activation of AMP-activated protein kinase (AMPK) [95,96], alter phospholipid homeostasis [53], and perturb liver DNA methylation [32,33]. It remains to be determined whether these mechanisms, or others not yet defined, connect the elevated SAM to impaired oxidative metabolism in GNMT-null mice.

5. CONCLUSION

Loss of GNMT impairs oxidative metabolism to promote liver steatosis via both SAM-dependent and SAM-independent actions. The decreased *in vivo* citric acid cycle flux occurs through mechanisms that are independent of the excess SAM. In contrast, gluconeogenesis and respiratory chain function are impaired by higher SAM. The SAM-dependent decline in oxidative metabolism is linked to dysregulated folate cycle and one-carbon donor metabolism.

AUTHOR CONTRIBUTIONS

C.C.H. and F.I.R.: Conceptualization, methodology, formal analysis, investigation, writing—review and editing—and visualization. C.C.H.: Writing—original draft—and supervision.

ACKNOWLEDGEMENTS

The authors thank the Vanderbilt University Medical Center Lipid Core (NIH DK059637 and DK020593) for completing the lipid measurements and Peter Crawford for helpful conversations. The authors are grateful to the Masonic Cancer Center Analytical Biochemistry shared resource at the University of Minnesota (NIH P30 CA77598) for access to GC—MS instrumentation. BioRender was used to create figure illustrations.

CONFLICT OF INTEREST

The authors declare no conflicts of interest, financial or otherwise.

REFERENCES

[1] Chalasani, N., Younossi, Z., Lavine, J.E., Diehl, A.M., Brunt, E.M., Cusi, K., et al., 2012. The diagnosis and management of non-alcoholic fatty liver disease: practice Guideline by the American Association for the Study of Liver Diseases. American College of Gastroenterology, and the American Gastroenterological Association Hepatology 55:2005—2023.

[2] Younossi, Z.M., Koenig, A.B., Abdelatif, D., Fazel, Y., Henry, L., Wymer, M., 2016. Global epidemiology of nonalcoholic fatty liver disease-Meta-analytic assessment of prevalence, incidence, and outcomes. Hepatology 64:73—84.

[3] Younossi, Z., Tacke, F., Arrese, M., Chander Sharma, B., Mostafa, I., Bugianesi, E., et al., 2019. Global perspectives on nonalcoholic fatty liver disease and nonalcoholic steatohepatitis. Hepatology 69:2672—2682.

[4] Rinella, M.E., 2015. Nonalcoholic fatty liver disease: a systematic review. JAMA : The Journal of the American Medical Association 313:2263—2273.

[5] Williams, C.D., Stengel, J., Asike, M.I., Torres, D.M., Shaw, J., Contreras, M., et al., 2011. Prevalence of nonalcoholic fatty liver disease and nonalcoholic steatohepatitis among a largely middle-aged population utilizing ultrasound and liver biopsy: a prospective study. Gastroenterology 140:124—131.

[6] Friedman, S.L., Neuschwander-Tetri, B.A., Rinella, M., Sanyal, A.J., 2018. Mechanisms of NAFLD development and therapeutic strategies. Nature Medicine 24:908—922.

[7] Sunny, N.E., Bril, F., Cusi, K., 2017. Mitochondrial adaptation in nonalcoholic fatty liver disease: novel mechanisms and treatment strategies trends in endocrinology and metabolism. Trends in Endocrinology and Metabolism 28: 250—260.

[8] Sunny, N.E., Parks, E.J., Browning, J.D., Burgess, S.C., 2011. Excessive hepatic mitochondrial TCA cycle and gluconeogenesis in humans with nonalcoholic fatty liver disease. Cell Metabolism 14:804—810.

[9] Fletcher, J.A., Deja, S., Satapati, S., Fu, X., Burgess, S.C., Browning, J.D., 2019. Impaired ketogenesis and increased acetyl-CoA oxidation promote hyperglycemia in human fatty liver. JCI Insight 5.

[10] Naguib, G., Morris, N., Yang, S., Fryzek, N., Haynes-Williams, V., Huang, W.A., et al., 2020. Dietary fatty acid oxidation is decreased in nonalcoholic fatty liver disease: a palmitate breath test study Liver. Bar International Series 40:590—597.

[11] Perez-Carreras, M., Del Hoyo, P., Martin, M.A., Rubio, J.C., Martin, A., Castellano, G., et al., 2003. Defective hepatic mitochondrial respiratory chain in patients with nonalcoholic steatohepatitis. Hepatology 38:999—1007.

[12] Koliaki, C., Szendroedi, J., Kaul, K., Jelenik, T., Nowotny, P., Jankowiak, F., et al., 2015. Adaptation of hepatic mitochondrial function in humans with nonalcoholic fatty liver is lost in steatohepatitis Cell. Metabolism 21:739—746.

[13] Cortez-Pinto, H., Chatham, J., Chacko, V.P., Arnold, C., Rashid, A., Diehl, A.M., 1999. Alterations in liver ATP homeostasis in human nonalcoholic steatohepatitis: a pilot study. JAMA : The Journal of the American Medical Association 282:1659—1664.

[14] Pierantonelli, I., Svegliati-Baroni, G., 2019. Nonalcoholic fatty liver disease: basic pathogenetic mechanisms in the progression from NAFLD to. NASH Transplantation 103:e1—e13.

[15] Liao, Y.J., Chen, T.L., Lee, T.S., Wang, H.A., Wang, C.K., Liao, L.Y., et al., 2012. Glycine N-methyltransferase deficiency affects Niemann-Pick type C2 protein stability and regulates hepatic cholesterol homeostasis. Molecular Medicine 18:412—422.

[16] Borowa-Mazgaj, B., de Conti, A., Tryndyak, V., Steward, C.R., Jimenez, L., Melnyk, S., et al., 2019. Gene expression and DNA methylation alterations in the Glycine N-methyltransferase gene in diet-induced nonalcoholic fatty liver disease-associated carcinogenesis. Toxicological Sciences 170:273—282.

[17] Fernandez-Tussy, P., Fernandez-Ramos, D., Lopitz-Otsoa, F., Simon, J., Barbier-Torres, L., Gomez-Santos, B., et al., 2019. miR-873-5p targets mitochondrial GNMT-Complex II interface contributing to non-alcoholic fatty liver disease. Molecular Metabolism 29:40—54.

[18] Huang, J.W., Chen, C.J., Yen, C.H., Chen, Y.A., Liu, Y.P., 2019. Loss of Glycine N-methyltransferase associates with angiopoietin-like protein 8 expression in high fat-diet-fed mice. International Journal of Molecular Sciences 20.

[19] Pogribny, I.P., Dreval, K., Kindrat, I., Melnyk, S., Jimenez, L., de Conti, A., et al., 2018. Epigenetically mediated inhibition of S-adenosylhomocysteine hydrolase and the associated dysregulation of 1-carbon metabolism in nonalcoholic steatohepatitis and hepatocellular carcinoma. The FASEB Journal 32:1591—1601.

[20] Pacana, T., Cazanave, S., Verdianelli, A., Patel, V., Min, H.K., Mirshahi, F., et al., 2015. Dysregulated hepatic methionine metabolism drives homocysteine elevation in diet-induced nonalcoholic fatty liver disease. PLoS One 10: e0136822.

[21] Martinez-Una, M., Varela-Rey, M., Mestre, D., Fernandez-Ares, L., Fresnedo, O., Fernandez-Ramos, D., et al., 2015. S-Adenosylmethionine increases circulating very-low density lipoprotein clearance in non-alcoholic fatty liver disease. Journal of Hepatology 62:673—681.

[22] Moylan, C.A., Pang, H., Dellinger, A., Suzuki, A., Garrett, M.E., Guy, C.D., et al., 2014. Hepatic gene expression profiles differentiate presymptomatic patients with mild versus severe nonalcoholic fatty liver disease. Hepatology 59:471—482.

[23] Mannisto, V., Kaminska, D., Karja, V., Tiainen, M., de Mello, V.D., Hanhineva, K., et al., 2019. Total liver phosphatidylcholine content associates with non-alcoholic steatohepatitis and glycine N-methyltransferase expression Liver. Bar International Series 39:1895—1905.

[24] Avila, M.A., Berasain, C., Torres, L., Martin-Duce, A., Corrales, F.J., Yang, H., et al., 2000. Reduced mRNA abundance of the main enzymes involved in methionine metabolism in human liver cirrhosis and hepatocellular carcinoma. Journal of Hepatology 33:907—914.

[25] Chen, Y.M., Shiu, J.Y., Tzeng, S.J., Shih, L.S., Chen, Y.J., Lui, W.Y., et al., 1998. Characterization of glycine-N-methyltransferase-gene expression in human hepatocellular carcinoma. International Journal of Cancer 75:787—793.

[26] Liu, H.H., Chen, K.H., Shih, Y.P., Lui, W.Y., Wong, F.H., Chen, Y.M., 2003. Characterization of reduced expression of glycine N-methyltransferase in cancerous hepatic tissues using two newly developed monoclonal antibodies. Journal of Biomedical Science 10:87—97.

[27] Lu, S.C., Mato, J.M., 2012. S-adenosylmethionine in liver health, injury, and cancer. Physiological Reviews 92:1515—1542.

[28] Hughey, C.C., Trefts, E., Bracy, D.P., James, F.D., Donahue, E.P., Wasserman, D.H., 2018. Glycine N-methyltransferase deletion in mice diverts carbon flux from gluconeogenesis to pathways that utilize excess methionine cycle intermediates. Journal of Biological Chemistry 293:11944—11954.

[29] Hughey, C.C., James, F.D., Wang, Z., Goelzer, M., Wasserman, D.H., 2019. Dysregulated transmethylation leading to hepatocellular carcinoma compromises redox homeostasis and glucose formation Mol Metab.

[30] Luka, Z., Capdevila, A., Mato, J.M., Wagner, C., 2006. A glycine N-methyltransferase knockout mouse model for humans with deficiency of this enzyme Transgenic. Res: Anthropology and Aesthetics 15:393—397.

[31] Liu, S.P., Li, Y.S., Chen, Y.J., Chiang, E.P., Li, A.F., Lee, Y.H., et al., 2007. Glycine N-methyltransferase-/- mice develop chronic hepatitis and glycogen storage disease in the liver. Hepatology 46:1413—1425.

[32] Martinez-Chantar, M.L., Vazquez-Chantada, M., Ariz, U., Martinez, N., Varela, M., Luka, Z., et al., 2008. Loss of the glycine N-methyltransferase gene leads to steatosis and hepatocellular carcinoma in mice. Hepatology 47: 1191—1199.

[33] Liao, Y.J., Liu, S.P., Lee, C.M., Yen, C.H., Chuang, P.C., Chen, C.Y., et al., 2009. Characterization of a glycine N-methyltransferase gene knockout mouse model for hepatocellular carcinoma: implications of the gender disparity in liver cancer susceptibility. International Journal of Cancer 124:816—826.

[34] Liu, S.P., Li, Y.S., Lee, C.M., Yen, C.H., Liao, Y.J., Huang, S.F., et al., 2011. Higher susceptibility to aflatoxin B(1)-related hepatocellular carcinoma in glycine N-methyltransferase knockout mice. International Journal of Cancer 128:511—523.

[35] Ayala, J.E., Bracy, D.P., Malabanan, C., James, F.D., Ansari, T., Fueger, P.T., et al., 2011. Hyperinsulinemic-euglycemic clamps in conscious, unrestrained mice Journal of visualized experiments. JoVE.

[36] Hughey, C.C., James, F.D., Bracy, D.P., Donahue, E.P., Young, J.D., Viollet, B., et al., 2017. Loss of hepatic AMP-activated protein kinase impedes the rate of glycogenolysis but not gluconeogenic fluxes in exercising mice. Journal of Biological Chemistry.

[37] Hasenour, C.M., Wall, M.L., Ridley, D.E., Hughey, C.C., James, F.D., Wasserman, D.H., et al., 2015. Mass spectrometry-based microassay of (2) H and (13)C plasma glucose labeling to quantify liver metabolic fluxes in vivo. American Journal of Physiology. Endocrinology and Metabolism 309: E191—E203.

[38] Soga, T., Heiger, D.N., 2000. Amino acid analysis by capillary electrophoresis electrospray ionization mass spectrometry. Analytical Chemistry 72:1236—1241.

[39] Soga, T., Ohashi, Y., Ueno, Y., Naraoka, H., Tomita, M., Nishioka, T., 2003. Quantitative metabolome analysis using capillary electrophoresis mass spectrometry. Journal of Proteome Research 2:488—494.

[40] Soga, T., Ueno, Y., Naraoka, H., Ohashi, Y., Tomita, M., Nishioka, T., 2002. Simultaneous determination of anionic intermediates for Bacillus subtilis metabolic pathways by capillary electrophoresis electrospray ionization mass spectrometry. Analytical Chemistry 74:2233—2239.

[41] Sugimoto, M., Wong, D.T., Hirayama, A., Soga, T., Tomita, M., 2010. Capillary electrophoresis mass spectrometry-based saliva metabolomics identified oral, breast and pancreatic cancer-specific profiles. Metabolomics 6:78—95.

[42] Trefts, E., Hughey, C.C., Lantier, L., Lark, D.S., Boyd, K.L., Pozzi, A., et al., 2019. Energy metabolism couples hepatocyte integrin-linked kinase to liver glucoregulation and the postabsorptive response of mice in an age-dependent manner. American Journal of Physiology. Endocrinology and Metabolism.

[43] Chan, T.M., Exton, J.H., 1976. A rapid method for the determination of glycogen content and radioactivity in small quantities of tissue or isolated hepatocytes. Analytical Biochemistry 71:96—105.

[44] Hasenour, C.M., Ridley, D.E., Hughey, C.C., James, F.D., Donahue, E.P., Shearer, J., et al., 2014. 5-Aminoimidazole-4-carboxamide-1-beta-D-ribofuranoside (AICAR) effect on glucose production, but not energy metabolism, is independent of hepatic AMPK in vivo. Journal of Biological Chemistry 289: 5950—5959.

[45] Hughey, C.C., Johnsen, V.L., Ma, L., James, F.D., Young, P.P., Wasserman, D.H., et al., 2012. Mesenchymal stem cell transplantation for the infarcted heart: a role in minimizing abnormalities in cardiac-specific energy metabolism. American Journal of Physiology. Endocrinology and Metabolism 302:E163—E172.

[46] Wang, Y.C., Chen, Y.M., Lin, Y.J., Liu, S.P., Chiang, E.P., 2011. GNMT expression increases hepatic folate contents and folate-dependent methionine synthase-mediated homocysteine remethylation. Molecular Medicine 17: 486—494.

[47] Wang, Y.C., Lin, W.L., Lin, Y.J., Tang, F.Y., Chen, Y.M., Chiang, E.P., 2014. A novel role of the tumor suppressor GNMT in cellular defense against DNA damage. International Journal of Cancer 134:799—810.

[48] Swanson, D.A., Liu, M.L., Baker, P.J., Garrett, L., Stitzel, M., Wu, J., et al., 2001. Targeted disruption of the methionine synthase gene in mice. Molecular and Cellular Biology 21:1058–1065.

[49] Matthews, R.G., Drummond, J.T., 1990. Providing one-carbon units for biological methylations: mechanistic studies on serine hydroxymethyltransferase, methylenetetrahydrofolate reductase, and methyltetrahydrofolate-homocysteine methyltransferase. Chemical Reviews 90:1275–1290.

[50] Kutzbach, C., Stokstad, E.L., 1971. Mammalian methylenetetrahydrofolate reductase. Partial purification, properties, and inhibition by S-adenosylmethionine. Biochimica et Biophysica Acta 250:459–477.

[51] Yamada, K., Strahler, J.R., Andrews, P.C., Matthews, R.G., 2005. Regulation of human methylenetetrahydrofolate reductase by phosphorylation. Proceedings of the National Academy of Sciences of the United States of America 102: 10454–10459.

[52] Xiu, Y., Field, M.S., 2020. The roles of mitochondrial folate metabolism in supporting mitochondrial DNA synthesis, oxidative phosphorylation, and cellular function. Current Developments in Nutrition 4 nzaa153.

[53] Martinez-Una, M., Varela-Rey, M., Cano, A., Fernandez-Ares, L., Beraza, N., Aurrekoetxea, I., et al., 2013. Excess S-adenosylmethionine reroutes phosphatidylethanolamine towards phosphatidylcholine and triglyceride synthesis. Hepatology 58:1296–1305.

[54] Liao, Y.J., Lee, T.S., Twu, Y.C., Hsu, S.M., Yang, C.P., Wang, C.K., et al., 2016. Glycine N-methyltransferase deficiency in female mice impairs insulin signaling and promotes gluconeogenesis by modulating the PI3K/Akt pathway in the liver. Journal of Biomedical Science 23:69.

[55] Miyazaki, M., Kim, Y.C., Gray-Keller, M.P., Attie, A.D., Ntambi, J.M., 2000. The biosynthesis of hepatic cholesterol esters and triglycerides is impaired in mice with a disruption of the gene for stearoyl-CoA desaturase 1. Journal of Biological Chemistry 275:30132–30138.

[56] Paton, C.M., Ntambi, J.M., 2009. Biochemical and physiological function of stearoyl-CoA desaturase. American Journal of Physiology. Endocrinology and Metabolism 297:E28–E37.

[57] Zubiete-Franco, I., Garcia-Rodriguez, J.L., Martinez-Una, M., Martinez-Lopez, N., Woodhoo, A., Juan, V.G., et al., 2016. Methionine and S-adenosylmethionine levels are critical regulators of PP2A activity modulating lipophagy during steatosis. Journal of Hepatology 64:409–418.

[58] Adeva-Andany, M.M., Gonzalez-Lucan, M., Donapetry-Garcia, C., Fernandez-Fernandez, C., Ameneiros-Rodriguez, E., 2016. Glycogen metabolism in humans. BBA Clinical 5:85–100.

[59] Pissios, P., 2017. Nicotinamide N-methyltransferase: more than a vitamin B3 clearance. Enzyme Trends in Endocrinology and Metabolism: Trends in Endocrinology and Metabolism 28:340–353.

[60] Burgess, S.C., He, T., Yan, Z., Lindner, J., Sherry, A.D., Malloy, C.R., et al., 2007. Cytosolic phosphoenolpyruvate carboxykinase does not solely control the rate of hepatic gluconeogenesis in the intact mouse liver. Cell Metabolism 5:313–320.

[61] Burgess, S.C., Hausler, N., Merritt, M., Jeffrey, F.M., Storey, C., Milde, A., et al., 2004. Impaired tricarboxylic acid cycle activity in mouse livers lacking cytosolic phosphoenolpyruvate carboxykinase. Journal of Biological Chemistry 279:48941–48949.

[62] She, P., Shiota, M., Shelton, K.D., Chalkley, R., Postic, C., Magnuson, M.A., 2000. Phosphoenolpyruvate carboxykinase is necessary for the integration of hepatic energy metabolism. Molecular and Cellular Biology 20:6508–6517.

[63] Shi, H., Fang, R., Li, Y., Li, L., Zhang, W., Wang, H., et al., 2016. The oncoprotein HBXIP suppresses gluconeogenesis through modulating PCK1 to enhance the growth of hepatoma cells Cancer. Letture 382:147–156.

[64] Bian, X.L., Chen, H.Z., Yang, P.B., Li, Y.P., Zhang, F.N., Zhang, J.Y., et al., 2017. Nur77 suppresses hepatocellular carcinoma via switching glucose metabolism toward gluconeogenesis through attenuating phosphoenolpyruvate carboxykinase sumoylation. Nature Communications 8:14420.

[65] Tuo, L., Xiang, J., Pan, X., Gao, Q., Zhang, G., Yang, Y., et al., 2018. PCK1 downregulation promotes TXNRD1 expression and hepatoma cell growth via the Nrf2/Keap1 pathway. Frontiers in Oncology 8:611.

[66] Tang, Y., Zhang, Y., Wang, C., Sun, Z., Li, L., Cheng, S., et al., 2018. Overexpression of PCK1 gene antagonizes hepatocellular carcinoma through the activation of gluconeogenesis and suppression of glycolysis pathways. Cellular Physiology and Biochemistry 47:344–355.

[67] Liu, M.X., Jin, L., Sun, S.J., Liu, P., Feng, X., Cheng, Z.L., et al., 2018. Metabolic reprogramming by PCK1 promotes TCA cataplerosis, oxidative stress and apoptosis in liver cancer cells and suppresses hepatocellular carcinoma. Oncogene 37:1637–1653.

[68] Hasek, B.E., Boudreau, A., Shin, J., Feng, D., Hulver, M., Van, N.T., et al., 2013. Remodeling the integration of lipid metabolism between liver and adipose tissue by dietary methionine restriction in rats. Diabetes 62:3362–3372.

[69] Malloy, V.L., Perrone, C.E., Mattocks, D.A., Ables, G.P., Caliendo, N.S., Orentreich, D.S., et al., 2013. Methionine restriction prevents the progression of hepatic steatosis in leptin-deficient obese mice. Metabolism 62: 1651–1661.

[70] Patil, Y.N., Dille, K.N., Burk, D.H., Cortez, C.C., Gettys, T.W., 2015. Cellular and molecular remodeling of inguinal adipose tissue mitochondria by dietary methionine restriction. The Journal of Nutritional Biochemistry 26: 1235–1247.

[71] Gomez, A., Gomez, J., Lopez Torres, M., Naudi, A., Mota-Martorell, N., Pamplona, R., et al., 2015. Cysteine dietary supplementation reverses the decrease in mitochondrial ROS production at complex I induced by methionine restriction. Journal of Bioenergetics and Biomembranes 47:199–208.

[72] Sanchez-Roman, I., Gomez, A., Perez, I., Sanchez, C., Suarez, H., Naudi, A., et al., 2012. Effects of aging and methionine restriction applied at old age on ROS generation and oxidative damage in rat liver mitochondria. Biogerontology 13:399–411.

[73] Caro, P., Gomez, J., Lopez-Torres, M., Sanchez, I., Naudi, A., Jove, M., et al., 2008. Forty percent and eighty percent methionine restriction decrease mitochondrial ROS generation and oxidative stress in rat liver. Biogerontology 9:183–196.

[74] Sanz, A., Caro, P., Ayala, V., Portero-Otin, M., Pamplona, R., Barja, G., 2006. Methionine restriction decreases mitochondrial oxygen radical generation and leak as well as oxidative damage to mitochondrial DNA and proteins. The FASEB Journal 20:1064–1073.

[75] Pettit, A.P., Jonsson, W.O., Bargoud, A.R., Mirek, E.T., Peelor 3rd, F.F., Wang, Y., et al., 2017. Dietary methionine restriction regulates liver protein synthesis and gene expression independently of eukaryotic initiation factor 2 phosphorylation in mice. Journal of Nutrition 147:1031–1040.

[76] Jonsson, W.O., Margolies, N.S., Mirek, E.T., Zhang, Q., Linden, M.A., Hill, C.M., et al., 2021. Physiologic responses to dietary sulfur amino acid restriction in mice are influenced by Atf4 status and biological sex. Journal of Nutrition 151:785–799.

[77] Cook, R.J., Wagner, C., 1984. Glycine N-methyltransferase is a folate binding protein of rat liver cytosol. Proceedings of the National Academy of Sciences of the United States of America 81:3631–3634.

[78] Chang, C.M., Yu, C.C., Lu, H.T., Chou, Y.F., Huang, R.F., 2007. Folate deprivation promotes mitochondrial oxidative decay: DNA large deletions, cytochrome c oxidase dysfunction, membrane depolarization and superoxide overproduction in rat liver. British Journal of Nutrition 97:855–863.

[79] Sid, V., Shang, Y., Siow, Y.L., Hewage, S.M., House, J.D., O, K., 2018. Folic acid supplementation attenuates chronic hepatic inflammation in high-fat diet fed mice. Lipids 53:709–716.

[80] Xin, F.Z., Zhao, Z.H., Zhang, R.N., Pan, Q., Gong, Z.Z., Sun, C., et al., 2020. Folic acid attenuates high-fat diet-induced steatohepatitis via deacetylase SIRT1-dependent restoration of PPARalpha World. Journal of Gastroenterology 26:2203–2220.

[81] Kim, H., Min, H., 2020. Folic acid supplementation prevents high fructose-induced non-alcoholic fatty liver disease by activating the AMPK and LKB1 signaling pathways. Nutrition and Research Practice 14:309—321.
[82] Fang, H., Stone, K.P., Ghosh, S., Forney, L.A., Gettys, T.W., 2021. The role of reduced methionine in mediating the metabolic responses to protein restriction using different sources of protein. Nutrients 13.
[83] Fang, H., Stone, K.P., Ghosh, S., Forney, L.A., Sims, L.C., Vincik, L., et al., 2021. Hepatic Nfe2l2 is not an essential mediator of the metabolic phenotype produced by dietary methionine restriction. Nutrients 13.
[84] Fang, H., Stone, K.P., Forney, L.A., Sims, L.C., Gutierrez, G.C., Ghosh, S., et al., 2021. Implementation of dietary methionine restriction using casein after selective. Oxidative Deletion of Methionine iScience 24:102470.
[85] Stone, K.P., Ghosh, S., Kovalik, J.P., Orgeron, M., Wanders, D., Sims, L.C., et al., 2021. The acute transcriptional responses to dietary methionine restriction are triggered by inhibition of ternary complex formation and linked to Erk1/2, mTOR, and ATF4. Scientific Reports 11:3765.
[86] Forney, L.A., Fang, H., Sims, L.C., Stone, K.P., Vincik, L.Y., Vick, A.M., et al., 2020. Dietary methionine restriction signals to the brain through fibroblast growth factor 21 to regulate energy balance and remodeling of adipose tissue obesity. Silver Spring) 28:1912—1921.
[87] Ghosh, S., Forney, L.A., Wanders, D., Stone, K.P., Gettys, T.W., 2017. An integrative analysis of tissue-specific transcriptomic and metabolomic responses to short-term dietary methionine restriction in mice. PLoS One 12: e0177513.
[88] Forney, L.A., Wanders, D., Stone, K.P., Pierse, A., Gettys, T.W., 2017. Concentration-dependent linkage of dietary methionine restriction to the components of its metabolic phenotype obesity. Silver Spring) 25:730—738.
[89] Wanders, D., Forney, L.A., Stone, K.P., Burk, D.H., Pierse, A., Gettys, T.W., 2017. FGF21 mediates the thermogenic and insulin-sensitizing effects of dietary methionine restriction but not its effects on hepatic lipid metabolism. Diabetes 66:858—867.
[90] Wanders, D., Stone, K.P., Forney, L.A., Cortez, C.C., Dille, K.N., Simon, J., et al., 2016. Role of GCN2-independent signaling through a noncanonical PERK/NRF2 pathway in the physiological responses to dietary methionine restriction. Diabetes 65:1499—1510.
[91] Zhou, X., Han, D., Xu, R., Wu, H., Qu, C., Wang, F., et al., 2016. Glycine protects against high sucrose and high fat-induced non-alcoholic steatohepatitis in rats. Oncotarget 7:80223—80237.
[92] Rom, O., Liu, Y., Liu, Z., Zhao, Y., Wu, J., Ghrayeb, A., et al., 2020. Glycine-based treatment ameliorates NAFLD by modulating fatty acid oxidation, glutathione synthesis, and the gut microbiome. Science Translational Medicine 12.
[93] Takashima, S., Ikejima, K., Arai, K., Yokokawa, J., Kon, K., Yamashina, S., et al., 2016. Glycine prevents metabolic steatohepatitis in diabetic KK-Ay mice through modulation of hepatic innate immunity. American Journal of Physiology - Gastrointestinal and Liver Physiology 311:G1105—G1113.
[94] Sim, W.C., Yin, H.Q., Choi, H.S., Choi, Y.J., Kwak, H.C., Kim, S.K., et al., 2015. L-serine supplementation attenuates alcoholic fatty liver by enhancing homocysteine metabolism in mice and rats. Journal of Nutrition 145:260—267.
[95] Varela-Rey, M., Fernandez-Ramos, D., Martinez-Lopez, N., Embade, N., Gomez-Santos, L., Beraza, N., et al., 2009. Impaired liver regeneration in mice lacking glycine N-methyltransferase. Hepatology 50:443—452.
[96] Martinez-Chantar, M.L., Vazquez-Chantada, M., Garnacho, M., Latasa, M.U., Varela-Rey, M., Dotor, J., et al., 2006. S-adenosylmethionine regulates cytoplasmic HuR via AMP-activated kinase. Gastroenterology 131:223—232.

